Emergent Materials (2024) 7:103–131
https://doi.org/10.1007/s42247-023-00576-y

REVIEW

Spinel ferrites for resistive random access memory applications

Ketankumar Gayakvad[1,6] · Kaushik Somdatta[2] · Vikas Mathe[3] · Tukaram Dongale[4] · Madhuri W[5] · Ketaki Patankar[6,7]

Received: 11 July 2023 / Accepted: 19 October 2023 / Published online: 22 November 2023
© The Author(s) 2023

Abstract
Cutting edge science and technology needs high quality data storage devices for their applications in artificial intelligence and digital industries. Resistive random access memory (RRAM) is an emerging nonvolatile memory used for recording and reproducing the digital information. Earlier studies on RRAM applications suggest that spinel ferrite is a potential material. We envisage that the spinel ferrite prepared by a particular route, namely spin coating, will in future optimize the essential parameters for optimal functioning of RRAM. An assertion to our assumptions, few researchers have already obtained important findings for spin coated spinel ferrites. Spin coated spinel ferrites, namely zinc ferrite, nickel ferrite, cobalt ferrite and mixed spinel ferrites, have been investigated for their applications as switching layers in RRAM devices. Particularly, spin coated cobalt ferrite, nickel ferrite and doped nickel ferrite were widely used as resistive switching layers. However, it is noticed that there is a tremendous scope for synthesis and resistive switching characterization of spin coated pure and doped zinc ferrite. Proper doping of special element into spinel ferrite can enhance the resistive switching performance of RRAM devices. Insertion of nano structures and metal layers within switching layer uplifts the performance of spin coated spinel ferrite-based RRAM devices. Active layer in RRAM device synthesized by spin coating technique exhibited good resistive switching properties, namely retention of 10^3 to 10^5 s, endurance in the range of 10^2 to 22,500 cycles and memory window of 10^2 to 10^6. This review article accounts for the optimized parameters obtained especially for the spinel ferrite-based active material synthesized by spin coating justifying the results with appropriate theory. A good co-relation between synthesis parameters and the RRAM functional parameter is separately discussed at the end of review article.

Keywords Spinel ferrite · Spin coating · Artificial intelligence · RRAM · Neuromorphic computing · Hardware security

1 Introduction

The 21st century is ruled by artificial intelligence and digital technology. The era of artificial intelligence (AI) and digital world demand high quality data storage devices for their applications in emerging fields of modern science and technology [1, 2]. These emerging fields are blockchain and cryptography [3, 4], microprocessor and micro controller [5, 6], in-Memory Computing [7, 8], internet of things (IoT) [9, 10], neuromorphic vision sensors [11, 12], neuromorphic computing [13, 14], modern space technology [15, 16], medical diagnosis [17, 18], genomic sequencing [19, 20], radio frequency communication [21, 22] and digital processing [23, 24]. The digital data is being processed and recorded in the binary language of zeros' and ones. As per literature survey, it seems that approximately 0.3 zetta byte (1 zetta byte=10^9 tera byte) world's data was stored in digital form during 2007. After that, 33 zetta byte of world's data was newly stored in the year 2018. As per the recent estimation, around 87.5 zetta byte data will be generated by 2025. This will be approximately 50 percent of predicated data during the year 2025 [25]. Thus, rapid rise in the generation of digital data requires good quality data storage devices. The increasing demand of data storage capacity is as shown in Fig. 1.

In the above view, entire focus is now on synthesizing and characterizing novel spinel ferrites for memory applications. Much research in recent years has focussed on semiconductor-based flash memories to serve the purpose of recording and reproducing the digital data [26, 27]. But, flash memories are finding limitations when scaling down to nanoscale [28]. Under miniaturization of flash memories, the problem of leakage current arises and becomes domi-

✉ Ketankumar Gayakvad
ketankumar@somaiya.edu

Extended author information available on the last page of the article

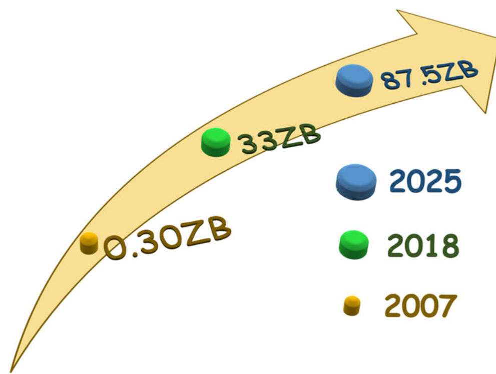

Fig. 1 Memory storage demand

nant [29]. According to Moore's law, miniaturization has its intrinsic limit because of technical complexity [30]. Nevertheless, flash memories are accompanied with challenges like high operating power, low operating speed and less durability [31]. To overcome these challenges associated with flash memories, memristive effect-based emerging nonvolatile random access memories (RAMs), namely spin transfer torque magnetic random access memory (STT-MRAM) [32], ferroelectric random access memory (FRAM) [33, 34], phase change random access memory (PCRAM) [35, 36] and resistive random access memory (RRAM) [37, 38] are widely explored. These memories are having peculiar properties, namely fast operating speed, low power consumption, high data storage density, high scalability and long retention [8, 39, 40]. The typical types of emerging nonvolatile RAMs' and their comparison are respectively shown in Figs. 2 and 3. Out of these four mentioned memories, RRAM finds distinct place for itself due to its peculiar and excellent performance parameters. The comparison among these four nonvolatile memories is as mentioned in Fig. 3.

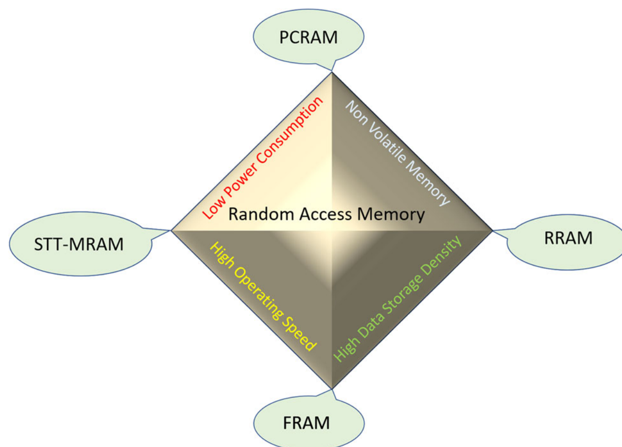

Fig. 2 Random access memory (RAM) types

RRAM possesses good complementary metal-oxide semiconductor (CMOS) integration, data retention and scalability as shown in Fig. 3. Data retention is the unique and distinguished property of RRAM among all emerging memristive effect-based nonvolatile memories. Additionally, RRAM has attracted attention due to its simple device configuration, low power consumption, high processing speed, good retention time, high endurance and excellent memory window [41, 42]. Therefore, various efforts across the globe are being put forth to bring RRAM device in the market. In the year 2008, HP Lab experimentally demonstrated memory storage characteristics using titanium dioxide as switching layer in $Pt/TiO_x/Pt$ RRAM device [43, 44]. Later on, various advanced and functional materials have been investigated as switching layers for RRAM devices [45, 46]. Nowadays, organic [47, 48], inorganic materials [49, 50], hybrid perovskites of organic and inorganics materials [51, 52], biomaterials [53] and magnetic materials [54, 55] are being widely employed as switching layer in RRAM devices. However, researchers found interest in exploring spinel ferrites as active materials for RRAM applications. The reasons are high resistivity [56, 57], good magnetic properties [58–61], high mechanical stability [62, 63] and simple crystal structure found in spinel ferrites. The structure of spinel ferrite is as shown in the Fig. 4 [64]: It is a closely packed cubic crystal consisting of eight units of MFe_2O_4 with a total of 56 ions. Out of these 56 ions, 32 are oxygen anions, 16 are iron cations and 8 are divalent cations. Because of availability of two different valence states of metal cations, namely +2 and +3, two types of crystallographic sites are present within the crystal structure of spinel ferrite. These are called as tetrahedral A site and octahedral B site. As shown in Fig. 4, tetrahedral A site is surrounded by four oxygen ions whereas octahedral B site is surrounded by six oxygen ions. The term spinel represents the cubic crystal structure having general chemical formula PQ_2O_4; where P is divalent cation and Q is trivalent cation. Therefore, spinel ferrite is considered as cubic crystal structure with Fe^{3+} as trivalent cation forming MFe_2O_4. Here, M is divalent metal cation and can be Mn^{+2}, Zn^{+2}, Co^{+2}, Ni^{+2}, Cu^{+2}, Mg^{+2} [65, 66]. These are termed as spinel because their chemical structure resembles with a naturally occurred spinel $MgAl_2O_4$. These ferrites exhibit good physio-chemical, physio-mechanical, good magneto-optic effect [67, 68], good spintronic characteristics [69, 70], thermal [71, 72], electrical [73, 74] and insulating properties. These remarkable properties make spinel ferrites suitable for their use as switching layers in RRAM devices. Recently, various techniques have been employed to synthesize switching layers of spinel ferrites. However, spin coated spinel ferrites are widely implemented and investigated for switching layers in RRAM devices [55,

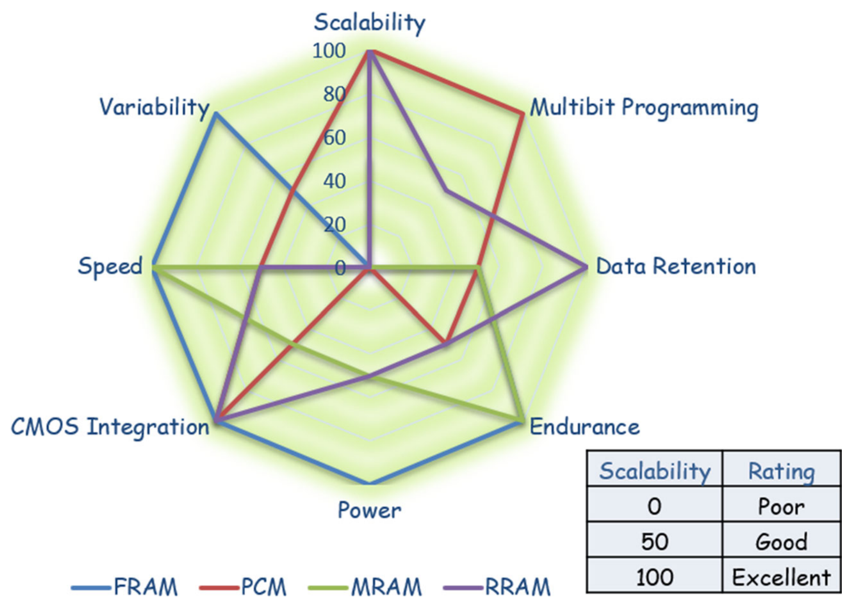

Fig. 3 Comparison among memristor-based random access memories

75–78]. Table 1 explores the chronological advancements [79–110] in spinel ferrite-based RRAM technology.

This review discusses the spin coated spinel ferrites as switching layers for resistive random access memory applications.

2 Theoretical overview, construction and performance of RRAM

2.1 Theoretical overview

RRAM functions on the basis resistive switching phenomenon. The theoretical behaviour of resistive switching is explained using characteristics of memristor [111]. Therefore, RRAM is also termed as memristor and its applications are generally called as memristive applications [112]. Memristor is the fourth fundamental circuit element in series with resistor, inductor and capacitor [113]. The relationship among electric charge, electric current, voltage, magnetic flux and their derivatives like capacitance (C), resistance (R), memristance (M) and inductance (L) is as shown in Fig. 5. Memristor was invented by L. Chua in 1971. It connects magnetic flux with electric charge. The term memristor represents memory plus resistor [114]. It is measured in memristance. It is a function of internal state variable x. Generally, memristive systems can be categorized into two types [75], namely,

1. Current controlled memristive system: Mathematically, it can be expressed as,

$$V_M = R(x, I_M, t)I_M(t)$$
$$\dot{x} = f(x, I_M, t)$$

2. Voltage controlled memristive system: The mathematical equation for the voltage controlled memristive system is given by,

$$I_M(t) = G(x, V_M, t)V_M(t)$$
$$\dot{x} = f(x, V_M, t)$$

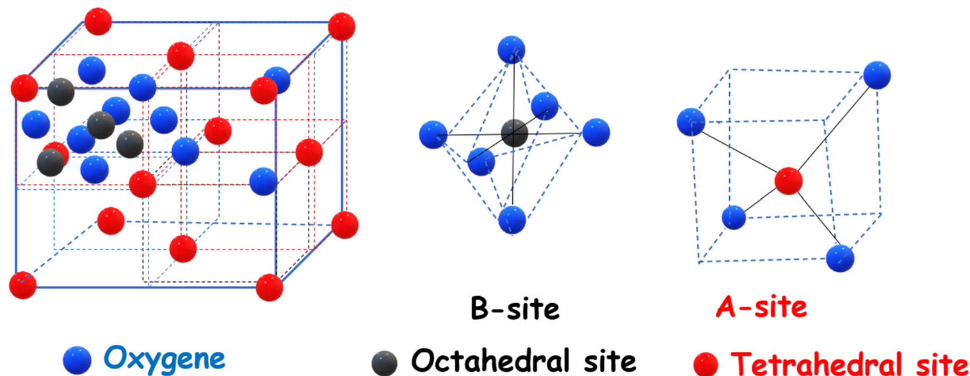

Fig. 4 Spinel ferrite crystal structure

Table 1 Chronological advancement in spinel ferrite-based RRAM research

Sr. No.	Year	M/I/M TE/IL/BE	Synthesis Route	Scientific Findings	Application	Ref.
1.	2011	Ag/NiFe_2O_4/SrTiO_3:Nb	Reactive co-sputtering	Resistive hysteresis in I-V of NFO/STON junction at room temperature	Nonvolatile Memory and Capacitor	[79]
2.	2012	Pt/NiFe_2O_4/Pt	Spin coating	URS	RRAM	[80]
3.	2012	Ag/ZnFe_2O_4/Pt	Spin coating	Bipolar and Tri-state URS	Multilevel and stable tri-state memories	[81]
4.	2014	Au/CoFe_2O_4/CoFe_2	Electro deposition	Investigation of novel conducting process for RRAM	Resistive Switching Memory	[82]
5.	2014	Pt/CoFe_2O_4/Pt	Spin coating	Conduction Mechanism of HRS and LRS is explored	Resistive Switching Memory	[83]
6.	2015	Pt/CoFe_2O_4/SrTiO_3:Nb/In	Pulsed Laser Deposition	Co-relation between magnetization and resistive switching is observed	Nonvolatile Multistate Memory and Magneto Electric Sensor	[84]
7.	2015	Pt/CoFe_2O_4/Pt	Spin coating	Investigation of Thickness dependence resistive switching	RRAM	[85]
8.	2016	Pt/$Co_{1-x}Cu_xFe_2O_4$/Pt	Spin coating	Cu impurity induces hopping process among Fe and Cu ions	RRAM	[86]
9.	2016	Pt/SnFe_2O_4/Pt	Spin coating	Effect of variation of spin coating cycles on stability of URS	RRAM	[87]
10.	2017	Ag/Cu doped ZnFe_2O_4/Au	Radio frequency magnetron sputtering	Assistance of Cu ions information of conductive filament	Next Generation Nonvolatile Memory applications	[88]
11.	2017	Pt/NiFe_2O_4/Pt	Solgel auto combustion	Polaron hopping mechanism with greater activation energy for smaller grain size	Spintronics	[89]
12.	2017	Pt/NiFe_2O_4/Nb:SrTiO_3	Pulsed Laser Deposition	Multilevel resistance states and associated magnetization is explained	Nonvolatile Multilevel Resistive Switching Memory	[90]
13.	2017	Pt/Ni$Fe_{2-x}Ce_xO_4$/Pt	Spin Coating	Rare earth doping enhances stability of resistive switching of memory device	Resistive Switching Memory	[91]
14.	2017	Pt/Ag NPs doped NiFe_2O_4/Pt	Spin coating	Effect of Ag Nanoparticles concentration on Resistive Switching characteristics of memory cell	Multifunctional electromagnetic devices	[92]

Table 1 continued

Chronological advancement of spin coated spinel ferrite-based RRAM research						
15.	2017	Al/CoFe_2O_4/FTO	Spin coating	Bipolar multifunctional Resistive Switching	RRAM	[93]
16.	2017	Ag/CoFe_2O_4/FTO	Spray pyrolysis	Bipolar with Analog Resistive Switching	synaptic devices	[75]
17.	2018	Ag/CoFe_2O_4/FTO	Spray pyrolysis	memcapacitance and meminductance properties are observed along with memresistance	RRAM	[94]
18.	2018	Pt/Gd doped NiFe_2O_4 /Pt	Spin coating	Resistive Switching and Magnetic characteristics can be improved by adding rare earth impurities in spinel ferrites	RRAM	[95]
19.	2018	Pt/Au-doped NiFe_2O_4/Pt	Spin coating	Influence of Au substitution on URS is observed	RRAM	[96]
20.	2018	Pt/Ag NPs doped NiFe_2O_4/Pt	Spin coating	Significance of Joule heating effect and electrochemical redox reaction is observed in BRS and URS	Resistive Switching Applications	[97]
21.	2018	Ti/ZnFe_2O_4/Pt Au/ZnFe_2O_4/Pt	Spin coating	Coexistence of URS and BRS	Nonvolatile Memory Applications	[98]
22.	2018	Pt/ZnFe_2O_4/Pt	Spin Coating	Nonpolar Resistive Switching is observed	Nonvolatile memory devices	[99]
23.	2018	Cu/CoFe_2O_4/Pt	Spin coating	Coexistence of ionic and metallic conducting filaments	Multistate and Multifunctional Resistive Switching Devices	[100]
24.	2019	Pt/$NiFe_{1.95}Cr_{0.05}O_4$/Pt	Spin coating	Cr doping reduces randomness information and rupture of conduction filament	Multistate logic resistive switching	[101]
25.	2019	Pt/$Ni_{0.5}Zn_{0.5}Fe_2O_4$/Pt	Radio frequency magnetron sputtering	Annealing effect on BRS memory is investigated	Nonvolatile memory applications	[102]
26.	2019	Pt/$Ni_{1-x}Cu_xFe_2O_4$/Pt	Spin coating	Conducting path can be controlled by substituting Cu^{2+} ions	Multifunctional device for RRAM	[103]
27.	2020	Al/NiFe_2O_4/FTO	Hydro thermal Synthesis	Forming Free BRS	RRAM	[104]
28.	2021	Ag/CoFe_2O_4/Pt	Spin coating	Compliance current controlled Resistive Switching and conduction mechanisms are explored	Volatile, Irreversible, And Non-volatile Memory applications	[105]

Table 1 continued

Chronological advancement of spin coated spinel ferrite-based RRAM research						
29.	2021	Pt/NiFe_2O_4/Pt or Au array/Pt	Spin coating	Enhancement of resistive switching parameters due to insertion of metal nano structures	RRAM	[106]
30.	2021	Pt/NiFe_2O_4/Pt	RF magnetron sputtering	Distiguishable Reversible and Reproducible Memory Window for an optimum active layer thickness	RRAM	[107]
31.	2021	Al/NiFe_2O_4/FTO	Co-ppt method followed by doctor blade	Bipolar Resistive Switching is observed	Resistive Memory	[76]
32.	2022	Pt/NFO/Pt Pt/NFO/Pt array/Pt Pt/NFO/Au array/Pt	Spin coating	Incorporation of array of Au/Pt nanostructures results in reduction of fluctuations in forming voltage and Enhancement in Uniformity of SET voltage	RRAM	[106]
33.	2022	W/ZnFe_2O_4/Pt	Pulsed Laser Deposition	Significance of optimum oxygen vacancies is required for resistive switching	Resistive Switching Applications	[108]
34.	2022	Pt/NiFe_2O_4/Ag NPs/NiFe_2O_4/Pt Pt/NiFe_2O_4/Cu NPs/NiFe_2O_4/Pt	Spin Coating	Incorporation of metal nanoparticle layer between multilayers of NiFe_2O_4 enhances resistive switching properties and reduces randomness information and rupture of conductive filament	Multi-layer Memory Device	[109]
35.	2022	Pt/NiFe_2O_4/Pt	Pulsed Laser Deposition	Coexistence of URS and BRS is observed	Multifunctional RRAM Device	[55]
36.	2022	Pt/$Ni_{0.5}Zn_{0.5}Fe_2O_4$/Pt	Pulsed Laser Deposition	Effect of active layer thickness on Resistive Switching Phenomena	Memristor	[54]
37.	2022	Cu/Co$Fe_{2-x}Ce_xO_4$/Cu	Co-precipitation Preparation of pellets	With Ce doping concentration, squareness of I-V hysteresis increases	RRAM	[78]
38.	2022	Ag/MFe_2O_4/Si (P++)	Spin Coating	Silicon (Si) can act as substrate as well as bottom electrode	Multifunctional Memory Device	[110]

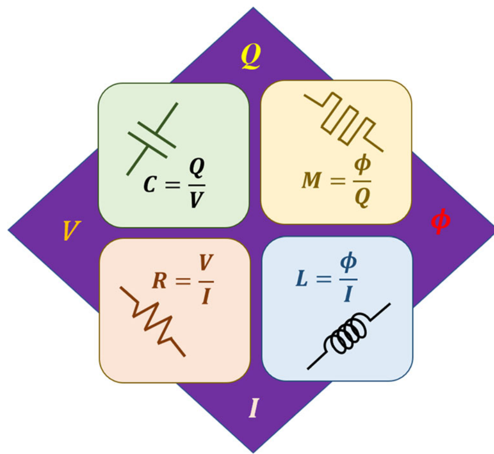

Fig. 5 Mathematical relationships among basic circuit elements

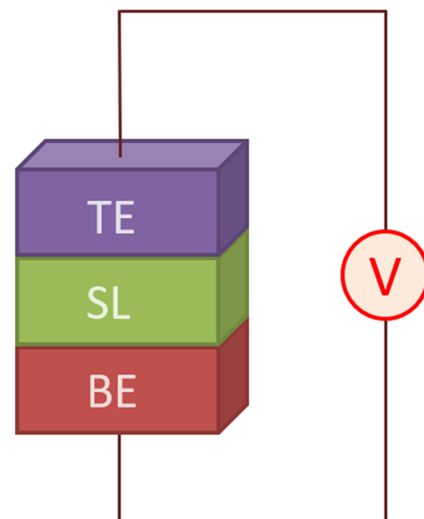

Fig. 6 Resistive random access memory cell configuration

Here, $V_M(t)$ and $I_M(t)$ represent the potential difference across the memristive device and current through the memristive device, x is a state variable, $\dot{x}$ is the rate of change of state variable with respect to time, R is the resistance due to memristor effect generally termed as memristance.

The internal state variable x is connected with migration of oxygen vacancies [111]. Thus, in case of oxide-based RRAM devices, the resistive switching mechanism is indirectly related with state variable x through the formation and breaking of conducting filament via oxygen vacancies. The generation and rupture of conducting path across the switching layer leads to resistive switching phenomenon which is the fundamental base of resistive random access memory device.

2.2 Construction of spinel ferrite-based RRAM

The typical configuration of the spinel ferrite-based RRAM device is consisting of a simple metal/spinel ferrite/metal (M/I/M) or TE/SL/BE stack as shown in Fig. 6.

The top and bottom metal layers in M/Spinel ferrite/M are generally termed as top electrode (TE) and bottom electrode (BE) whereas the spinel ferrite layer is termed as active material or switching layer (SL). The electrodes play an important role in the performance of the switching mechanism. So we have to discuss the type and nature of electrode material.

2.3 Types of top and bottom electrodes

2.3.1 Composition-based types of electrodes

On the basis of composition of electrodes, they typically classified into six types, namely,

1. **Oxides electrodes:**
   ITO [115, 116], FTO [117, 118], Nb:SrTiO_3 [119, 120], SrRuO_3 [121, 122],
   LaNiO_3 [123, 124], Al doped ZnO (AZO) [125, 126], Ga doped ZnO (GZO) [127, 128]
2. **Elementary electrodes:**
   Al [129–131], Au [132, 133], Ag [134, 135], Pd [136, 137], Ru [138, 139],
   Cr [140, 141], Co, Ni [142, 143], Cu [144, 145], Zr [146, 147], Nb [148, 149],
   Ta [150, 151], Ti [152, 153], Hf [154, 155], W [156, 157], Ir [158, 159]
3. **Alloy electrodes:**
   Cu-Ti [160, 161], Pt-Al [162, 163],Cu-Te [164, 165]
4. **Novel electrodes:**
   Carbon Nano Tube [166, 167], Graphene [168, 169]
5. **Nitrides electrodes:**
   Titanium nitride (TiN) [170, 171],Tantalum nitride (TaN) [172, 173],Tungsten nitride (WN) [174, 175]
6. **Silicon electrodes:**
   p-type Si [176, 177] and n-type Si [178, 179]

2.3.2 Electrochemical response-based types of electrodes

Depending upon contribution of electrode in terms of electrochemical performance during resistive switching phenomenon, electrodes are categorized into three types as listed below:

1. Electrochemically inert electrodes:
   Pt [180, 181], W [155], Ir [182], Pd [183], Co [184], Au [185]
2. Electrochemically active electrodes:
   Ag [186], Cu [187], Ni [155], Al [188], Ti [189], Ta [190], Hf [191], Zr [147]

3. Special purpose electrodes:
   FTO [192, 193], ITO [194, 195], n-Si [196, 197], p-Si [198, 199]

2.4 Performance of spinel ferrite as switching layer in RRAM

The switching layer (SL) made up of spinel ferrites can be switched between two quantized resistance states under the influence of externally applied unipolar or bipolar electric field. The quantized resistance states can be designated as high resistance state (HRS) and low resistance state (LRS). The HRS of RRAM device can be treated as logic 0 and the LRS as logic 1. The switching from LRS to HRS is termed as RESET whereas the switching from HRS to LRS is called as SET. In other words, we can store the data as logic 1 and logic 0 in RRAM device under the influence of externally applied unipolar or bipolar biasing. Thus, we can record the binary data in terms of cyclic switching of resistance states. This repeated switching of resistance states is generally termed as resistive switching cycle. The active material composition is a key parameter in the performance of resistive switching characteristics. So different compositions of active spinel ferrite material along with their performances are discussed.

2.4.1 Spin coated pure and doped cobalt ferrite for RRAM

The peculiar properties of $CoFe_2O_4$, namely, excellent mechanical stability [200, 201], remarkable thermal stability [202, 203], and good insulating property [204, 205], make $CoFe_2O_4$ eligible for its use in wide range of applications. Magnetic recording devices, supercapacitors [206], Lithium-Ion batteries [207], Gas Sensors [208], environmental [209], biomedical and petroleum industries [210, 211] and RRAM devices [77] are typical applications of cobalt ferrite. Spin coated thin film of $CoFe_2O_4$ shows excellent RRAM properties like good endurance, retention and large memory window [212]. The resistive switching properties and underlying valence change conduction mechanism of spin coated pure and doped cobalt ferrites are respectively tabulated in Tables 2 and 5. Wei Hu and co-authors [83] prepared spin coated nano structured cobalt ferrite thin film on Platinum substrate and hence fabricated Pt/$CoFe_2O_4$/Pt resistive switching device. From the cross-sectional scanning electron microscopy (SEM) image, the thickness of $CoFe_2O_4$ layer was found to be around 120 nm. For this thickness of switching layer, electroforming phenomenon is required to initiate resistive switching mechanism. The electroforming voltage of 4.2V accompanied with a compliance current of 3 mA was applied to investigate resistive switching properties. They observed highly reproducible and unipolar resistive switching cycles with good endurance (>100 cycles), retention (10^4) and memory window of 100 as listed in Sr. No. 1 of Table 2. They also studied HRS and LRS as a function of temperature and observed the ohmic conduction in LRS whereas Schottky emission and Pool-Frenkel emission (for higher voltage region) in HRS and concluded that the resistive switching mechanism follows Valence change resistive switching mechanism (Table 5). Millaty Mustaqima and co-workers [85] have studied the regulation parameters of the forming process and the SET voltage fluctuations of resistive switching cycles in spin coated $CoFe_2O_4$ switching layer of Pt/$CoFe_2O_4$/Pt RRAM device. They have optimized numbers of coats, thickness of switching layer and annealing temperature to get stable and uniform resistive switching characteristics. Corresponding to annealing temperatures 500 degree celsius and 700 degree celsius, they fabricated two RRAM devices, namely Pt/$CoFe_2O_4$-500/Pt and Pt/$CoFe_2O_4$-700/Pt. Here, $CoFe_2O_4$-500 indicates that the switching layer is annealed at 500 degree celsius and Pt/$CoFe_2O_4$-700/Pt is annealed at 700 degree celsius. They found reproducible URS in both devices. However, the reproducibility and uniformity are much better in the device Pt/$CoFe_2O_4$-700/Pt as compared to Pt/$CoFe_2O_4$-500/Pt. Furthermore, forming voltage for Pt/$CoFe_2O_4$-500/Pt RRAM device was much larger (20V) as compared to Pt/$CoFe_2O_4$-700/Pt (5V). The smaller forming voltage in the Pt/$CoFe_2O_4$-700/Pt device as compared to Pt/$CoFe_2O_4$-500/Pt RRAM device may be due to increased oxygen vacancies and smaller grain boundaries. They also observed smaller fluctuation in V_{SET} of Pt/$CoFe_2O_4$-700/Pt as compared to Pt/$CoFe_2O_4$-500/Pt. Thus, higher the concentration of oxygen vacancies and highly directional grain boundaries facilitate the generation of conducting filament resulting in a lowering of forming voltage and less randomness in V_{SET}. Additionally, they investigated the effect of thickness of switching layer on resistive switching characteristics. With increase in thickness, initial resistance of the switching layer also increases. Therefore, forming free (FF) switching is possible for lower thickness whereas forming required (FR) is found in comparatively thick switching layer. The main advantage of forming free process is the reduction in power consumption due to lower forming voltage and good resistive switching stability due to the less fluctuation in V_{SET}. Sandeep Munjal and Neeraj Khare [93] explored the resistive switching mechanism in Al/$CoFe_2O_4$/FTO RRAM device. They co-related resistive switching with the magnetization. They observed the valence change mechanism for bipolar resistive switching cycle. The coupling of resistive switching with magnetic modulation of the Al/$CoFe_2O_4$/FTO RRAM device may find scope in multifunctional RRAM devices. In another publication [100], they found multilevel resistive switching accompanied with magnetic switching in Cu/$CoFe_2O_4$/Pt RRAM device. They proposed the electrochemical metallization (ECM) and the Valence Change Mechanism (VCM)

Table 2 Spin coated pure and doped cobalt ferrite as switching layer in RRAM

Sr. No.	TE/SL/BE configuration	Thickness of Switching Layer nm	RS Mode	FF/FR	V_F V	I_{compl} mA	$\frac{R_{HRS}}{R_{LRS}}$	Endurance cycles	Retention sec	Ref
1	$Pt/CoFe_2O_4/Pt$	120	URS	FR	4.2	3	10^2	> 100	10^4	[83]
2	$Pt/CoFe_2O_4/Pt$	100	URS	FF and FR	20(CFO-500) 5(CFO-700)	-	-	-	-	[85]
3	$Al/CoFe_2O_4$/FTO	200	BRS	FR	6.5	-	10^3	200	10^4	[93]
4	Cu/CoFe_2O_4/Pt	100	BRS	FR	3	-	-	500	10^5	[100]
5	Ag/$CoFe_2O_4$/Pt	100	BRS	FR	2.5	100 10 0.1	10^2 to 10^6	> 500	$> 10^3$	[105]
6	Pt/$Co_{1-x}Cu_xFe_2O_4$/Pt	152	URS	FR	-	2	10^3	-	>3500	[86]

FF: Forming Free, FR: Forming Required, V_F is Forming Voltage, I_{compl} is compliance current

to explain the multilevel resistive and magnetic switching. The co-existence of metallic and ionic conducting filaments was observed in the Cu/CoFe_2O_4/Pt RRAM device. They proposed that the conducting filament is made up of oxygen vacancies and Cu atoms in Cu/CoFe_2O_4/Pt. In another publication [105], Sandeep Munjal and Neeraj Khare studied compliance current dependent volatile and nonvolatile memory effect in Ag/CoFe_2O_4/Pt RRAM device. For smaller value of $I_{cc} = 10^{-4}$A, the device showed volatile memory characteristics whereas for larger value of $I_{cc} = 10^{-1}$A, the device exhibited nonvolatile nature of resistive switching. They have proposed ECM and VCM for lower I_{cc} and higher I_{cc} respectively. Zhao Xiahou and his team [86] studied the Cu ion substitution influence on the resistive switching properties of spin coated CoFe_2O_4 switching layer of Pt/$Co_{1-x}Cu_xFe_2O_4$/Pt RRAM device. They observed the hopping phenomenon between the Fe ions and Cu ions. This results in significant improvement in electrical conductivity. For 60 percent Cu ion doping, the hopping process is observed to be most active and hence less fluctuations were observed in V_{SET}. Thus, addition of Cu doping into the switching layer (cobalt ferrite) induces stability and uniformity of resistive switching cycles.

From Table 2, we can infer that Ag/$CoFe_2O_4$/Pt RRAM device exhibits bipolar resistive switching with endurance greater than 500 cycles and retention greater than 1000s. This memory device exhibits excellent memory window among all cobalt ferrite-based switching layers (10^2 to 10^6) and the lowest forming voltage around 2.5 V.

2.4.2 Spin coated pure and doped nickel ferrite for RRAM

Spin coated thin film of NiFe_2O_4exhibits good chemical and thermal stability [213], electrical resistivity [214] and mechanical stability [215]. Because of these remarkable properties, spin coated pure and doped nickel ferrites are widely employed in modern technology. Wei Hu and co-workers [80] reported resistive switching parameters of Pt/NiFe_2O_4/Pt RRAM device. They observed URS cycle of retention of 10^5 second, memory window of 10^3 and endurance of around 22,500 cycles. Each cycle consists of SET and RESET. The SET state of the Pt/NiFe_2O_4/Pt RRAM device resulted because of conducting filament generation across the switching layer. The conducting filament is made up of oxygen vacancies and reduced cations. Due to joule heating and redox reaction, the conducting filament would break and the RRAM device returns to RESET state.

Aize Hao and his team [91] observed the effect of rare earth element Ce substitution into the switching layer of Pt/Ni$Fe_{2-x}Ce_xO_4$/Pt. They observed significant enhancement in the directionality of formation of conducting filament across the switching layer of RRAM device. In fact, the Ce substitution in thin film of NiFe_2O_4 assists the process of formation of conducting filament via increased concentration of oxygen vacancies in the switching layer. Oxygen vacancies minimize the multiple conducting paths as well as support the formation of conductive filament across the switching layer. Thus, highly directional conducting filament is possible and hence the random formation and breaking of conducting filament is minimized which leads to highly uniform switching cycles. Consequently, resistive switching properties improve significantly on account of addition of rare earth element Ce into the NiFe_2O_4.

Aize Hao, Muhammad Ismail and co-workers [92] reported the effect of Ag substitution in the switching layer of Pt/Ag doped NiFe_2O_4/Pt RRAM device. The doping of Ag is responsible for observed coexistence of Unipolar Resistive Switching (URS) and Bipolar Resistive Switching (BRS). Thus, valence change mechanism and electrochemical metallization both contribute towards the coexistence of URS and BRS. Presence of URS and BRS modes is useful for reliable resistive switching cycles in terms of electric energy expenditure. The device exhibited higher memory window and comparatively rapid switching performance. The Ag substitution increases the directionality of conducting filament in the switching layer. Therefore, uniform and stable resistive switching cycles are observed due to incorporation of Ag nanoparticles into the switching layer.

Aize Hao, Muhammad Ismail and co-workers [95] have studied the effect of Gd doping in nickel ferrite thin film-based switching layer of Pt/Ni$Fe_{2-x}Gd_xO_4$/Pt RRAM device. Accordingly, resistive switching of Pt/NiFe_2O_4/Pt is greatly influenced by addition of Gd into switching layer. It was observed that conducting path is generated at the site of impurity and the cycle of formation and breaking of conducting path continues with the assistance of proper amount of Gd. Thus, uniform and steady switching cycles with good retention were reported for x=0.075 into Pt/Ni$Fe_{2-x}Gd_xO_4$/Pt. However, over doping of Gd in NiFe_2O_4 switching layer adversely affected the performance of resistive switching cycles.

Aize Hao, Muhammad Ismail, Shuai He and co-workers [96] observed the influence of substitution of Au in NiFe_2O_4 thin film of Pt/Au-doped NiFe_2O_4 /Pt RRAM device. Accordingly, Au increases oxygen vacancies within active layer that causes the decrease in energy required to form the conducting filament at the Au site. Thus, proper addition of Au in NiFe_2O_4 thin film enhances the quality of resistive switching cycles of Pt/Au-doped NiFe_2O_4 /Pt RRAM device in terms of endurance, retention and memory window. The 1 percent Au doping results in optimum performance of the RRAM device. It shows good memory window (10^2–10^3), retention of 10^5 second and endurance of around 10^3 cycles.

Aize Hao, Muhammad Ismail, Shuai He and co-workers [97] found the coexistence of unipolar resistive switching and bipolar resistive switching in Pt/0.5 percent Ag NP doped

NiFe_2O_4 /Pt RRAM device. The 0.5 percent doping of Ag nanoparticles into the switching layer of Pt/0.5 percent Ag NP doped NiFe_2O_4 /Pt RRAM device has significantly improved the quality of resistive switching cycles. Aize Hao, Dianzeng Jia and co-workers [101] have done the manipulation of resistive switching in Pt/Ni$Fe_{1.95}Cr_{0.05}O_4$/Pt RRAM device using externally applied electric field. Cr-impurities would increase uniformity and stability in the switching parameters by minimizing the randomness in formation and breaking of conducting filament. On the same line, Aize Hao, Dianzeng Jia and the team [103] have checked the effect of Cu^{2+} doping into NiFe_2O_4 thin film. They observed fall down of forming voltage due to Cu^{2+} impurity. Proper amount of Cu^{2+} substitution leads to improved stability of resistive switching cycles. Cu^{2+} impurity in nickel ferrite gives direction to the conducting path and hence controls the resistive switching phenomena. Metal nanoparticle layers can be deposited above and below NiFe_2O_4 active layers to boost resistive switching performances. Shuting Wang and co-workers [109] prepared spin coated NiFe_2O_4 thin films and fabricated Pt/NFO/Ag NPs/NFO/Pt and Pt/NFO/Cu NPs/NFO/Pt RRAM device. They have inserted additional layers of metal nanoparticles, namely Ag and Cu, between switching layers NiFe_2O_4 thin films to form the RRAM devices. They found good command over the generation and breaking of conducting filament across the active layers due to the addition of layers of metal nanostructures. Recently, Jiacheng Li, Chuangye Yao and co-workers [106] inserted arrays of pyramid shaped Au/Pt nanostructures between switching layer and bottom electrode. The Au/Pt pyramid shaped nanostructure acts as the point of distorted electric field at the interface of switching layer and Au/Pt nanostructures. This causes temperature gradient within the switching layer. The temperature gradient minimizes the random growth conducting filament and maximizes the uniformity and stability of generation and breaking of conducting filament. This produces highly uniform resistive switching in Pt/NFO/Pt array/Pt and Pt/NFO/Au array/Pt RRAM devices as compared to Pt/NFO/Pt RRAM device. All these pure and doped nickel ferrite-based RRAM devices and their resistive switching properties are listed in Table 3.

2.4.3 Spin coated pure and doped zinc ferrite for RRAM

Zinc ferrite exhibits excellent chemical and mechanical hardness [216], thermal stability [217] and distinguished electrical characteristics [218]. Therefore, zinc ferrite is widely investigated for various applications, namely, gas sensors, DSSC electrode [219, 220], water purification [221], hyperthermia applications [222], ferrofluid [223, 224], photocatalyst [225, 226] and random access memory applications [88, 227]. Nowadays, spin coated zinc ferrite is widely investigated for switching layer of resistive random access memory device [98, 99, 102, 228]. Table 4 explores spin coated zinc ferrite as switching layer in terms of resistive switching parameters. Wei Hu, Xinman Chen and team [81] studied Ag/ZnFe_2O_4/Pt memory device. They investigated the dependency of conducting filament growth and decay on compliance current. With the increase in the magnitude of set compliance current, the single prominent conducting filament grows across the switching layer irrespective of surrounding incomplete branches of conducting filaments. This results in strong conducting filament which needs more energy to dissolve. Therefore, higher magnitude of current is required to break the conducting filament. Thus, comparatively higher reset current is needed to bring the RRAM device into RESET state. The SET-RESET-SET-RESET-..resistive switching cycle continues. They observed stable and reproducible bipolar resistive switching cycles as well as tri-state unipolar resistive switching performances. This type of memory device can be employed to fabricate multilevel and highly uniform tri-state memories. Muhammad Ismail, Aize Hao et al. [99] observed reversible transitions among four modes of nonpolar resistive switching in Pt/ZnFe_2O_4/Pt RRAM cell. During consecutive 200 cycles, the memristive device undergo each of four modes of nonpolar resistive switching after every 50 resistive switching cycles. During all modes of nonpolar resistive switching, SET and RESET process is governed by thermochemical reaction and joule heating respectively. They observed that the conducting filament formed during SET process of resistive switching cycle is due to thermochemical reaction of oxygen vacancies and metallic zinc atoms whereas, RESET process is the outcome joule heating during around the conducting filament. In another report by Muhammad Ismail, Aize Hao et al. [98] observed coexistence of unipolar resistive switching mode and bipolar resistive switching mode in Au/ZnFe_2O_4/Pt and Ti//ZnFe_2O_4/Pt RRAM devices. They have reported the effect of nature of top and bottom electrode material on resistive switching phenomenon. Depending upon the response to the externally applied electric bias, we can classify resistive switching cycles into various types, namely unipolar resistive switching (URS) cycles, bipolar resistive switching (BRS) cycles and nonpolar resistive switching cycles.

2.5 Resistive switching mechanism

2.5.1 Unipolar resistive switching cycle

If the resistive switching depends only on magnitude and independent of polarity of externally applied electric field, the switching is said to be unipolar resistive switching (URS) or symmetric switching [229].

The unipolar switching cycle is as shown in Fig. 7. Unipolar resistive switching cycle is generally observed in the RRAM device having both top and bottom electrodes

Table 3 Spin coated pure and doped nickel ferrite as switching layer in RRAM

Sr. No.	TE/SL/BE configuration	Thickness of Switching Layer nm	RS Mode	FF/FR	V_F V	I_{compl} mA	$\frac{R_{HRS}}{R_{LRS}}$	Endurance cycles	Retention second	Ref
1	Pt/$NiFe_2O_4/Pt$	350	URS	FR	-	10	10^3	22,500	10^5	[80]
2	Pt/Ce doped $NiFe_2O_4$/Pt	-	URS	FR	-	10	10^3	500	10^5	[91]
3	Pt/ Ag (0.5%) doped NiFe_2O_4/Pt	370	URS	FR	10	10	10^2	$> 10^3$	10^5	[92]
4	Pt/Gd doped $NiFe_2O_4$/Pt	330	URS	FR	-	10	$> 10^2$	> 500	10^5	[95]
5	Pt/Au-doped $NiFe_2O_4$/Pt	360	URS	FR	-	10	$10^2–10^3$	$> 10^3$	10^5	[96]
6	Pt/0.5 percent Ag NP doped $NiFe_2O_4$/Pt	360	URS BRS	FR	-	10	$> 10^2$	10^3	10^5	[97]
7	Pt/$NiFe_{1.95}Cr_{0.05}O_4$/Pt	-	URS	FR	10.04	-	10^2	-	10^5	[101]
8	Pt/Cu doped $NiFe_2O_4$/Pt	320	URS	FR	-	10	10^2	10^3	10^5	[103]
9	Pt/NFO/Ag NPs/NFO/Pt Pt/NFO/Cu NPs/NFO/Pt	-	URS	FR	-	10	$> 7 \times 10^2$	10^3	10^5	[109]
10	Pt/NFO/Pt Pt/NFO/Pt array/Pt Pt/NFO/Au array/Pt	110	BRS	FR	6.5	-	10^2	10^2	10^3	[106]

FF: Forming Free, FR: Forming Required, V_F is Forming Voltage, I_{compl} is compliance current

Table 4 Spin coated pure and doped zinc ferrite as switching layer in RRAM

Sr. No.	TE/SL/BE configuration	Thickness of Switching Layer nm	Resistive Switching Mode	FF/FR	V_F V	I_{compl} mA	$\frac{R_{HRS}}{R_{LRS}}$	Endurance cycles	Retention sec	Ref
1	Pt/$ZnFe_2O_4$/Pt	300	Nonpolar	FR	9	10	10^2	200	-	[99]
2	Ag/$ZnFe_2O_4$/Pt	200	URS and BRS	FR	3	1 10	10^3	800	-	[81]
3	Au/$ZnFe_2O_4$/Pt Ti/$ZnFe_2O_4$/Pt	-	URS BRS	FR	6.4	10	10^2	100	-	[98]

FF: Forming Free, FR: Forming Required, V_F is Forming Voltage, I_{compl} is compliance current

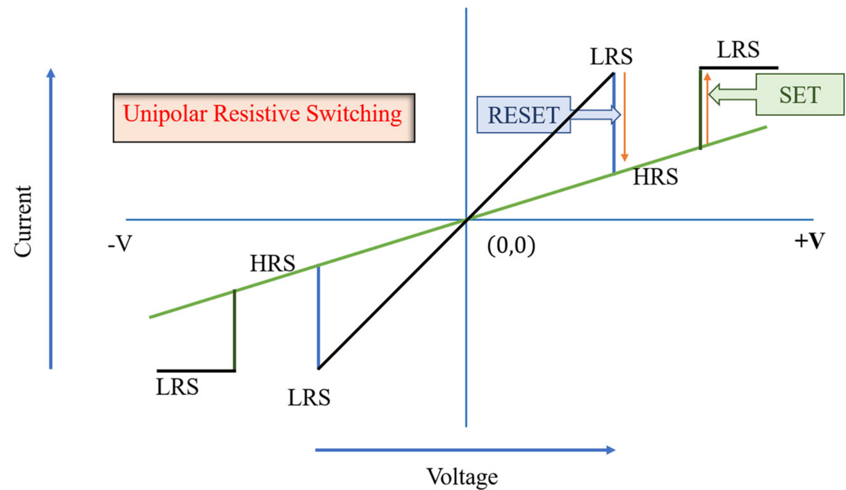

Fig. 7 Unipolar resistive switching cycle

of electrochemically inert material [230]. Top and bottom electrodes of Pt/NiFe_2O_4/Pt RRAM device are made of platinum (Pt). We can employ conducting filament theory to explain the unipolar resistive switching mechanism in case of Pt/NiFe_2O_4/Pt RRAM device [96].

As shown in Fig. 8(p), initially the RRAM device is in its pristine state. Under application of biasing voltage between top electrode (TE) and bottom electrode (BE) of Pt/$NiFe_2O_4$/Pt RRAM device, electroforming process takes place within the switching layer. The electroforming process generates oxygen vacancies and/or reduced metal ions. Thus, generated metal ions and oxygen vacancies start migration towards the bottom electrode (BE) under the application of electric biasing. The stacking of oxygen vacancies and/or metal ions forms the conducting path across the switching layer as shown in Fig. 8(q) and hence the RRAM device attains LRS. The LRS is featured by Ohmic conduction. Further increase in applied voltage tends to break conducting filament due to thermal heating (Fig. 8(r)). Therefore, the

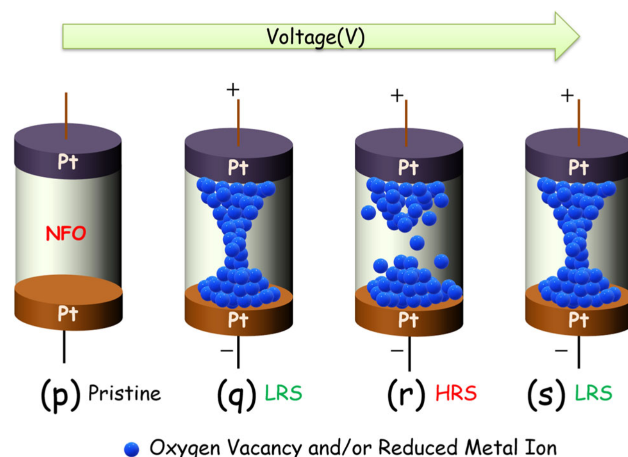

Fig. 8 Unipolar resistive switching in NiFe_2O_4 active layer

RRAM device switches to HRS. The HRS is dominated by Schottky and Pool-Frenkel Emission. This implies that oxygen vacancies and/or metal ions are still available within the active layer. Further increasing the magnitude of externally applied voltage, the oxygen vacancies and/or metal ions again form the conducting path across the switching layer and raise the device to LRS as shown in Fig. 8(s).

Thus, resistive switching of the Pt/$NiFe_2O_4$/Pt memristive device from HRS to LRS to HRS to LRS.....occurs, which is analogous to the switching of binary digits 0 to 1 to 0 to 1....

2.5.2 Bipolar resistive switching cycle

If the resistive switching depends on magnitude as well as polarity of externally applied electric field, the resistive switching is said to be bipolar resistive switching (BRS) or antisymmetric switching [231]. The bipolar resistive switching cycle is as shown in Fig. 9.

Typically, BRS occurs in the RRAM device whose one of the electrodes is electrochemically active and the counter electrode is electrochemically inert. In case of Al/NiFe_2O_4/FTO device, aluminium (Al) is electrochemically active metal whereas FTO is electrochemically inert electrode. The possible BRS mechanism in case of Al/NiFe_2O_4/FTO device can be understood with the help of Fig. 10 as follows [76].

Figure 10(α) shows pristine state of the NiFe_2O_4 switching layer in Al/NiFe_2O_4/FTO RRAM device. It is highly insulating and hence practically conducts no current until and unless the device is biased with required magnitude and polarity of electric voltage. The externally applied biasing induces electroforming process. The electroforming process generates oxygen vacancies near Top Electrode (TE)/$NiFe_2O_4$ interface. Under externally applied electric biasing, positive at top electrode (Al) and grounding at bot-

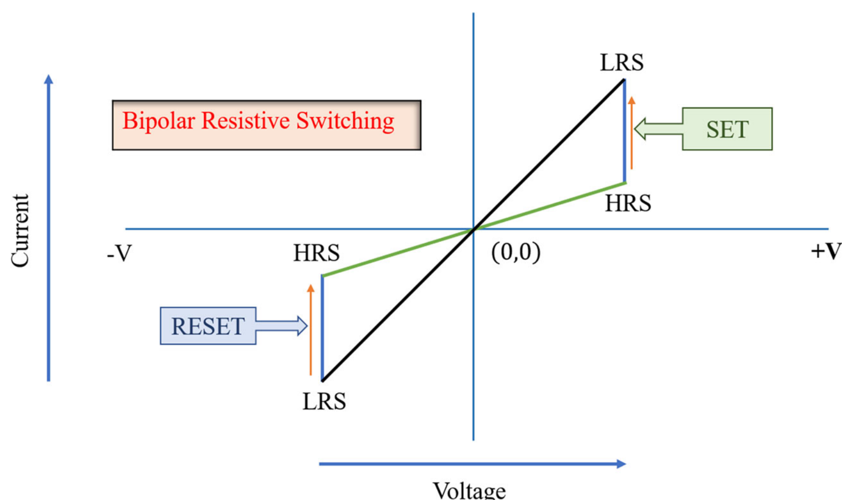

Fig. 9 Bipolar resistive switching cycle

tom electrode (FTO), an oxidation/reduction electrochemical reaction occurs within switching layer. The electrochemical reaction produces oxygen anions. Being negatively charged, oxygen anions start their journey towards the top electrode (Al). Meanwhile, positively charged Oxygen vacancies migrate towards the bottom electrode (FTO). During this phenomenon of migration of ions, the diffusion layer made of oxygen may be generated at the Al/$NiFe_2O_4$ interface. During low voltage positive biasing, the oxygen diffusion layer leads to the Schottky conduction as shown in Fig. 10(β). The electroforming process generates defects and traps sites in the switching layer of the RRAM device. The de-trapping of oxygen vacancies and/or electrons results in rapid growth of current at higher magnitude of positive voltage region (Fig. 10(γ)). This mechanism is generally referred to as a Pool-Frenkel conduction mechanism. The RRAM device since its SET voltage is +2V continues its LRS state until -2V.

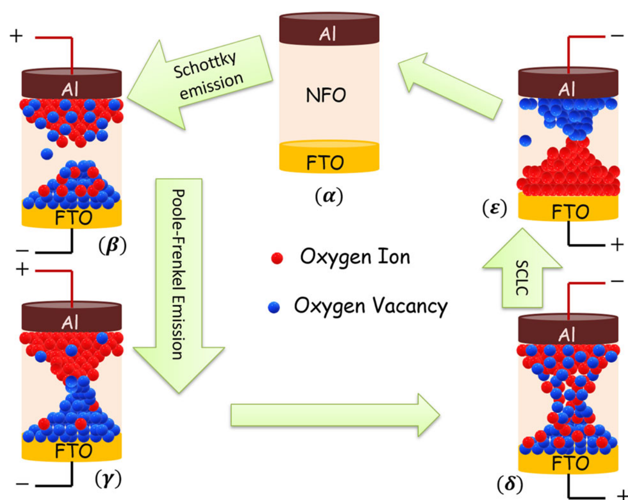

Fig. 10 Bipolar resistive switching in NiFe_2O_4 active layer

The generation of conductive filament (CF) in the switching layer (Fig. 10(δ)) leads to LRS of the device. But, as the applied voltage is varied from -2V to 0V, the device switches to HRS. However, the device shows the LRS because of narrow conducting filament as shown in Fig. 10(ϵ). Thus, trap assisted SCLC phenomena is responsible for LRS of the device. Further increase in the negative biasing at top electrode (Al) causes complete breakdown of conductive filament and hence the device attains the HRS. The switching of the Al/$NiFe_2O_4$/FTO RRAM device from HRS $\rightarrow$ LRS $\rightarrow$ HRS $\rightarrow$ LRS.....can be treated as switching from logic 0$\rightarrow$logic 1 $\rightarrow$ logic 0 $\rightarrow$ logic 1....

2.5.3 Nonpolar resistive switching cycles

Nonpolar resistive switching exhibits properties of both unipolar resistive switching and bipolar resistive switching [232]. Unipolar resistive switching and bipolar resistive switching both require external polarizing voltage to initiate resistive switching mechanism whereas nonpolar resistive switching does not consume voltage for polarization of switching layer and hence polarizing voltage is not needed. However, nonpolar resistive switching is characterized either by means of externally applied positive or negative electric biasing. Nonpolar resistive switching possesses advantages of both unipolar resistive switching as well as bipolar resistive switching [233]. There are four modes of resistive switching cycles. Out of these, two modes are belonging to URS and remaining two modes are of BRS. The mode of resistive switching cycle is governed by factors, namely, material of switching layer, top and bottom electrode material and biasing voltage. Various resistive switching mechanisms are proposed to comprehend underlying science of resistive switching mechanism in RRAM devices. The above different types of switching mechanisms were observed in different

spinel ferrite-based RRAM devices by earlier researchers. Their observations are tabulated in Tables 2, 3, and 4. Critical analysis of the tables suggests that among different materials synthesized by spin coating route, every material has its own unique properties. Therefore, every spinel ferrite is equally promising active material for RRAM applications. This is why, the review mainly focuses on spinel ferrite and that too in particular using the same synthesis route.

3 Scientific insights into the performance of RRAM

Resistive switching mechanism is mainly dependent on role of metal ion or cation of electrode, valence state of switching layer material and externally applied electric biasing. Accordingly, resistive switching in spinel ferrite-based switching layers of RRAM devices might be explained using the following phenomena, namely, valence change charge transfer phenomenon, thermochemical charge transfer phenomenon and electrochemical metallization phenomenon [234, 235].

3.1 Electrochemical metallization phenomenon

Electrochemical metallization mechanism mainly occurs in the RRAM device whose one of the electrodes is made of electrochemically active metal like nickel (Ni), copper (Cu), aluminium (Al), titanium (Ti) and silver (Ag) whereas the counter electrode is of electrochemically inert metal, namely platinum (Pt), gold (Au) and tungsten (W) [236]. Switching Layer for electrochemical metallization RRAM devices is generally made up of oxides like titanium dioxide (TiO_2), silicon dioxide (SiO_x), oxide of tungsten (WO_3) and oxide of Zirconium (ZrO_3) [237]. The electrodes play dominant role in electrochemical metallization supported RRAM devices. Active electrode generates the cation which entre into the switching layer of RRAM device [238]. Under the application of external electric field, the cation moves towards the counter electrode and get assembled. These assembled cations at counter electrode generate conducting filament which plays vital role in the switching of RRAM device from HRS to LRS and vice versa [239, 240]. Such types of cation-migration supported resistive switching are generally observed in electrochemical metallization memristors [237]. Thus, we can infer that the asymmetric combination of an electrochemically active electrode (Ag, Cu, Al, Ti or Ni) and an electrochemically inert electrode (Au, W, Pt) with suitable switching layer and a sufficient biasing voltage of proper polarity generates migration of cations from one electrode to counter electrode. The resistive random access memory based on this particular resistive switching mechanism is also known as conducting bridge random access memory or electrochemical metallization memory. The typical illustration of generation and breaking of conducting filament in electrochemical metallization memory device is as shown in Fig. 11 [241]. Initially, the RRAM device is in virgin state before application of external voltage as shown in Fig. 11(m). Once the external electric field is applied, formation and rupturing of conducting filament take place. Formation of conducting filament consists of the following stages, namely,

1. Oxidation at anode-switching layer interface: Under the influence of sufficient voltage between top and bottom electrodes, metal cations will be formed via oxidation reaction as shown in Fig. 11(n):
   $A \rightarrow A^{n+} + ne^-$
   Here, A is the element of anode material and n is the number of electrons which depends on the concentration of cations. Oxidation reaction is followed by the migration of metal cation across switching layer.
2. Migration of metal cation: Under the influence of externally applied electric bias, metal cation travel towards the inert electrode and undergo reduction process at switching layer-cathode interface as shown in Fig. 11(o).
3. Reduction at switching layer-cathode interface: $A^{n+} + ne^- \rightarrow A$

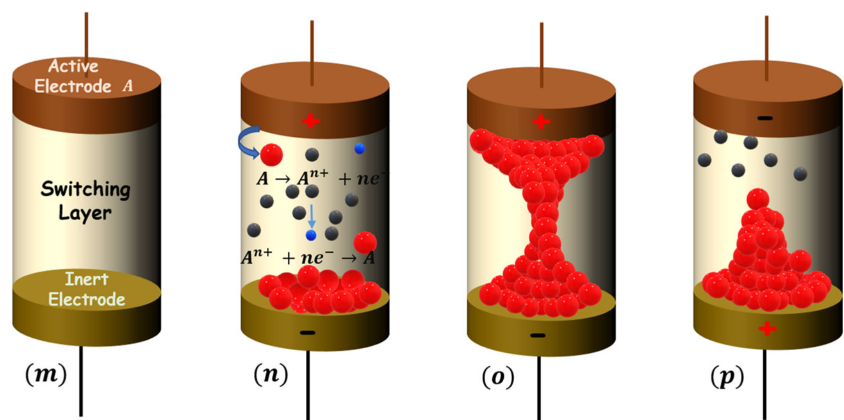

Fig. 11 ECM-based generation and breaking of conducting filament

Thus, reduction reaction causes accumulation of metal elements on the surface of counter electrode which leads to the generation of a conducting filament across the switching layer as shown in Fig. 11(o). This phenomenon corresponds to the SET process of the electrochemical metallization memory. The RRAM device is RESET with an application of externally applied voltage of the reverse polarity. This breaks the conducting filament and the RRAM device achieves the RESET state as shown in Fig. 11(p). Therefore, electrochemical metallization memories generally exhibit bipolar resistive switching.

In this way, SET and RESET of RRAM device continue in electrochemical metallization-based resistive random access memories. During SET process, current passes through the conductive filament and hence heat generated causing joule heating.

3.2 Thermochemical phenomenon

The temperature dependent resistive switching mechanism is popularly known as thermochemical mechanism. Most of resistive random access memories based on transition metal oxides as switching layers are following thermochemical mechanism. The thermochemical mechanism is strongly depending on temperature rise generated due to the current passing across the switching layer. The rise in temperature depends linearly on instantaneous power dissipation. We have,

$$T = T_0 + \alpha IV$$

Here, T_0 is room temperature, α is steady-state thermal coefficient, I is current and V is voltage. The rise in temperature as a result of joule heating causes a phase change in transition metal oxides. Such phase transitions among crystal structures of the same material cause switching between LRS and HRS [39, 242]. Another possibility is generation and breaking of conducting filament due to joule heating. Typically, such processes are usually observed in unipolar resistive switching devices.

3.3 Valence change phenomenon

Valence change resistive switching is mainly observed if the switching layer of RRAM device is made up of metal oxides like titanium dioxide, cobalt iron oxides, nickel iron oxides and zinc iron oxides. Spinel ferrites are metal iron oxides and hence exhibit valence change mechanism during resistive switching. Table 5 enlists valence change mechanism in spin coated spinel ferrite-based SL of RRAM devices. Here, LRS represents low resistance state and HRS is for high resistance state. Metal oxides are mainly reservoir of plenty of defects generally termed as oxygens vacancies. These oxygen vacancies incorporate electrons into the switching layer. Under the influence of externally applied electric biasing, electrons migrate towards anode and oxygen vacancies towards cathode. During the journey of oxygen vacancies through switching layer, they may encounter with metal ions. This causes change in oxidation state of metal ions and hence induces change in electrical conductivity across switching layer. Thus, change in the electrical conductivity causes change among resistance states which leads to resistive switching phenomenon. Therefore, we can infer that resistive switching is governed by change in the valency of metal ions which contributes towards electrical conductivity within the switching layer of RRAM device. The conduction of electric charge via conducting filament follows various conduction mechanisms, namely Ohmic conduction, Schottky emission, Pool-Frenkel (P-F) emission, Trap assisted tunneling, Nearest Neighbor Hopping conduction, Fowler Nordheim (F-N) Tunneling, Direct Tunneling, Space Charge Limited Conduction (SCLC) and Ionic Conduction. LRS and HRS of spin coated spinel ferrite switching layer may undergo various conduction mechanisms. The detailed conduction mechanisms are tabulated in Table 5 and the mathematical expressions for all these conduction mechanisms in terms of current density J as a function of electric field intensity E and temperature T are listed in Table 6. Thus, electrochemical metallization memory (ECM), thermochemical memory (TCM) and valence change memory (VCM) are typical types of memories belonging to cationic and ionic movement-based RRAM devices. These RRAM devices are widely employed in cutting edge random access memory-based applications. The results obtained by earlier researchers for their measured performance parameters are summarized and compared in the given tables. The separate tables are maintained for covering chronological survey, correlation with theory and particular material performance.

4 RRAM applications in diverse fields

RRAM devices are used in various fields, namely artificial intelligence, neuromorphic computing and hardware security.

4.1 Artificial intelligence

John Mc Carthy, a mathematics professor coined the term artificial intelligence in 1955 [244]. Artificial intelligence uses RRAM device for diverse applications due to its high density data storage capacity, fast read and write processing speed, low energy consumption, good resistive switching performance and better nonvolatility [245, 246]. These RRAM

Table 5 Valence change mechanism in spinel ferrite-based switching layer (SL) layer of RRAM device

Sr. No	TE/SL/BE	LRS	HRS	Reference
1	Pt/$CoFe_2O_4$/Pt	Ohmic	0.0–0.3V-Ohmic conduction 0.4–1.3V-Schottky emission 1.4–1.8V-Pool-Frenkel emission	[83]
2	$Pt/CoFe_2O_4/Pt$	Ohmic	$<$ 0.7V -Ohmic conduction $>$ 0.7V -Trap Free Space Charge Limited	[85]
3	$Al/CoFe_2O_4/FTO$	Ohmic	0.08–0.41V-Schottky emission 0.41–0.71V-Pool-Frenkel Conduction	[93]
4	Pt/$NiFe_2O_4$/Pt	Ohmic	0.0–0.5V-Ohmic conduction 0.5-V_{SET}-Schottky emission	[80]
5	Pt/Ce doped $NiFe_2O_4$/Pt	Ohmic	$<$ 1.3V -Ohmic Conduction $>$ 1.3V -Schottky emission	[91]
6	Pt/ Ag-NP doped $NiFe_2O_4$/Pt	Ohmic	$<$ 1.0V-Ohmic conduction $>$ 1.0V-Schottky emission	[92]
7	Pt/Gd doped $NiFe_2O_4$/Pt	Ohmic	$<$ 1.0V -Ohmic conduction $>$ 1.0V -Schottky emission	[95]
8	Pt/Au-doped $NiFe_2O_4$/Pt	Ohmic	Low field-Ohmic conduction High field-Schottky emission	[96]
9	Pt/Ag doped $NiFe_2O_4$/Pt	Ohmic	For URS and BRS:Schottky emission	[97]
10	Pt/$NiFe_{1.95}Cr_{0.05}O_4$/Pt	Ohmic	Low voltage-Ohmic conduction High voltage-Schottky emission	[101]
11	Pt/Cu doped $NiFe_2O_4$/Pt	Ohmic	$<$ 1.0V -Ohmic conduction $>$ 1.0V -Schottky emission	[103]
12	Pt/NFO/Ag NPs/NFO/Pt Pt/NFO/Cu NPs/NFO/Pt	Ohmic	Low voltage-Ohmic conduction High voltage-Schottky emission	[109]
13	$Ag/(Co, Cu, Ni, Zn)Fe_2O_4/Si-p++$	Ohmic	Low voltage-Schottky emission Moderate voltage-Pool-Frenkel Conduction Higher voltage-SCLC	[110]
14	$Ag/ZnFe_2O_4/Pt$	Ohmic	0–0.3V -Ohmic conduction 0.3–1.6V -Child square law $>$1.6V-Trap Controlled SCLC	[81]
15	Pt/$ZnFe_2O_4$/Pt	Ohmic	Low voltage-Ohmic conduction Higher voltage-Schottky emission	[99]
16	Ti/$ZnFe_2O_4$/Pt	Ohmic	Low voltage-Ohmic conduction Higher voltage-Schottky emission	[98]

characteristics are widely employed in RRAM supported artificial intelligence. As shown in Fig. 12, robotics [247, 248], neuromorphic vision [249, 250], natural language processing [251, 252], cognitive computing [253, 254], big data [255, 256], speech recognition [257, 258], neural networks [259, 260] and machine learning [246, 261] are typical RRAM-based applications of artificial intelligence (Fig. 12).

4.2 Neuromorphic computing

RRAM devices exhibit properties analogous to characteristics required for brain's neural network, namely, analog resistive switching, synaptic weight, low energy consumption, computation in memory abilities and device scalability. Therefore, RRAM devices are employed in neuromorphic

Table 6 Mathematical expressions for conduction mechanisms of VCM [92, 95, 99, 243]

Sr. No	Conduction Mechanism	Current density	Current density as a function of electric field and temperature
1	Ohmic conduction	$J_{ohmic} = q\mu N_c E e^{-\frac{E_g}{2kT}}$	$J_{ohmic} \propto E$
2	Schottky emission	$J_{SE} = \frac{4\pi qmK^2}{h^3} T^2 e^{-\frac{q\psi_s}{kT}} e^{\frac{aE^{\frac{1}{2}}}{kT}}$	$J_{SE} \propto T^2 e^{\frac{\sqrt{E}}{T}}$
3	Pool-Frenkel (P-F) emission	$J_{PF} = \frac{(4\pi qmK^2)}{h^3} E e^{(\frac{\beta_{P-F}\sqrt{E}}{kT} - \frac{E_g}{kT})}$	$J_{PF} \propto E e^{\frac{\sqrt{E}}{T}}$
4	Fowler Nordhein (F-N) Tunneling	$J_{F-N} = \frac{q^2}{8\pi h\psi_T} E^2 e^{-\frac{8\pi\sqrt{2\pi m_T}}{3hE}\psi_T^{\frac{3}{2}}}$	$J_{FN} \propto E^2 e^{\frac{-1}{E}}$
5	Direct Tunneling	$J_{DT} = \frac{3.38\times 10^{10}}{\psi_T} E^2 e^{-\frac{0.69\psi_T^{\frac{3}{2}}}{E}}$	$J_{DT} \propto E^2 e^{-\frac{1}{E}}$
6	Ionic Conduction	$J_{ionic} \propto \frac{E}{T} e^{-\frac{\psi_{in}}{kT}}$	$J_{ionic} \propto \frac{E}{T} e^{-\frac{1}{T}}$
7	Nearest Neighbor Hopping	$J_{NNH} = \sigma_0 e^{-\frac{T_0}{T}E}$	$J_{NNH} \propto E e^{-\frac{1}{T}}$
8	Trap assisted tunneling	$J_{TAT} = A e^{-\frac{8\pi\sqrt{2qm^*}}{3hE}\phi_T^{\frac{3}{2}}}$	$J_{TAT} \propto e^{-\frac{1}{E}}$
9	Space Charge Limited Conduction (SCLC)	$J_{SCLC} = \frac{9}{8}\epsilon_i \mu\theta \frac{V^2}{d^3}$	$J_{SCLC} \propto E^2$

N_c is the density of states, μ is the mobility of electrons, ψ_T is the mean barrier height, ψ_{in} is the barrier energy height, ψ_s is the height of the potential barrier, β_{P-F} is a constant

sensors [262, 263], quantum computing [264, 265], neuromorphic photonic synapses [266, 267], medical diagnosis [17, 268], artificial synapses [269, 270], topological computing [271, 272], tactile receptor [273, 274] and neuromorphic vision [275, 276]. The typical neuromorphic computing applications are as shown in Fig. 13.

4.3 Hardware security

Hardware security uses RRAM devices for various applications as shown in Fig. 14, namely, random number generator [277, 278], intellectual property protection [279, 280], non-volatile security [281–283], secure key storage and physically unclonable functions (PUFs) [284–286]. Thus, RRAM devices exhibit diverse applications in cutting edge technology of artificial intelligence, neuromorphic computing and hardware security. Due to such diverse applications, various functional and novel materials, namely, primary oxides, binary oxides, graphene, bio materials and spinel structured magnetic materials generally termed as spinel ferrites have been studied for synthesizing switching layer of RRAM device. Spinel ferrites are good insulators and hence recently these materials have been widely investigated and researched to get the stable and uniform resistive switching cycles for RRAM devices (Fig. 14).

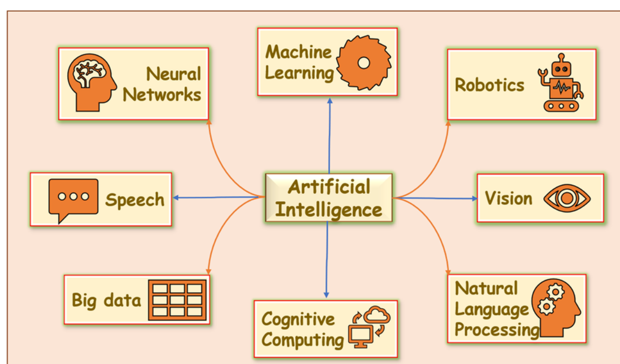

Fig. 12 Applications of artificial intelligence

5 Conclusion

The entire review article mainly focuses on spinel ferrite for RRAM applications. This paper communicates the required theory as well as construction and performance of spinel ferrites as active materials in RRAM applications. The different vital parts present in the RRAM are separately discussed and their influences on switching cycle is also discussed. The author has also systematically analysed the scientific phenomena envolve in the performance of RRAM. The novelty in the work lies in giving pictorial images that cover the working mechanism and scientific phenomena involved. The key findings on the research work earlier in this area are systematically surveyed and tabulated with all the important performance parameters in Tables 2, 3, 4, 5 and 6.

From this review, the author states that "Composition of spinel ferrites, types of synthesis route, amount, type of dopant used and types of electrode determine the performance of spinel ferrite as active material in RRAM". The literature survey done and the author impressions made together assert our hypothesis.

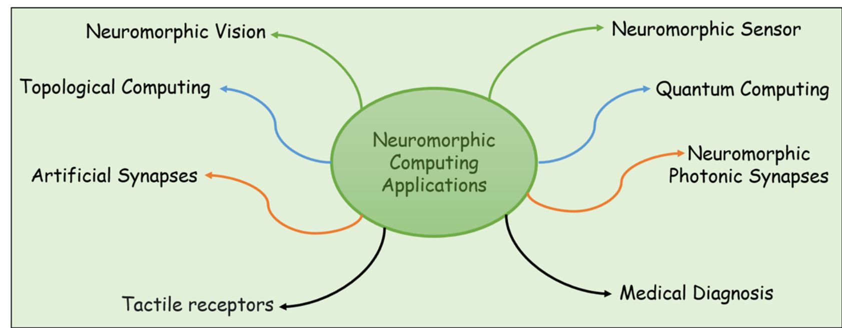

Fig. 13 Neuromorphic computing applications

This review article provides the guideline to the new researcher for exploring the basic spinel ferrite material using dopants having multivalent states. Future scope of research also provides the ready guidelines of strategies to be adopted while undertaking the research in this area. This strategies are given below:

1. Applying different compliance current across RRAM device.
2. Adding impurities into the switching layer.
3. Variation in concentration of impurities to be added into switching layer.
4. Insertion of additional layers of metal between switching layer and bottom/top electrode.
5. Addition of nanoparticles into the switching layer.
6. Variation in thickness of the switching layer.
7. Variation in annealing temperature of the switching layer.
8. Use of novel electrodes (CNT or graphene) as TE and BE of RRAM device for spinel ferrite-based switching layers of resistive switching memories.

Above strategies will definitely improve the quality of resistive switching cycles of RRAM devices in terms of endurance, retention, memory window, energy consumption, stability and uniformity of switching cycles. Based on these properties, it will be possible to design multifunctional RRAM devices for their applications in emerging trend of artificial intelligence and digital technology.

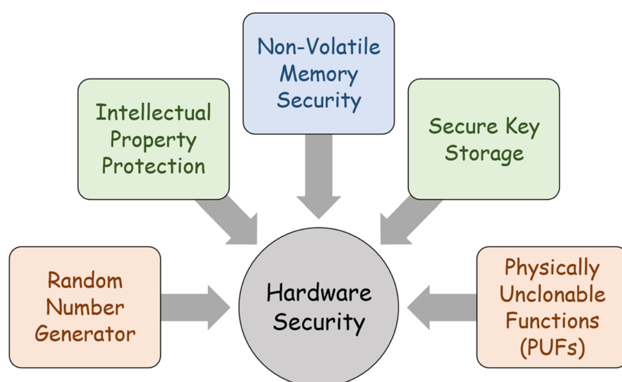

Fig. 14 Hardware security applications

Author contribution All authors contributed to the study conception and design. Material preparation, data collection and analysis were performed by Mr. Ketankumar Gayakvad and Dr. Ketaki Patankar. The first draft of the manuscript was written by Mr. Ketankumar Gayakvad and all authors commented on previous versions of the manuscript. All authors read and approved the final manuscript.

Data availability The authors declare that most of the data supporting the findings of this study are available within the papers at Google Scholar and IEEE database.

Declarations

Conflict of interest The authors declare no competing interests.

Open Access This article is licensed under a Creative Commons Attribution 4.0 International License, which permits use, sharing, adaptation, distribution and reproduction in any medium or format, as long as you give appropriate credit to the original author(s) and the source, provide a link to the Creative Commons licence, and indicate if changes were made. The images or other third party material in this article are included in the article's Creative Commons licence, unless indicated otherwise in a credit line to the material. If material is not included in the article's Creative Commons licence and your intended use is not permitted by statutory regulation or exceeds the permitted use, you will need to obtain permission directly from the copyright holder. To view a copy of this licence, visit http://creativecommons.org/licenses/by/4.0/.

References

1. H. Jeong, L. Shi, Memristor devices for neural networks. J. Phys. D Appl. Phys. **52**(2), 023003 (2018)
2. K. Humood, B. Mohammad, H. Abunahla, A. Azzam, On-chip tunable memristor-based flash-adc converter for artificial intelligence applications. IET Circ. Devices Syst. **14**(1), 107–114 (2020)
3. J. Yang, R. Lin, K. Zhou, Y. Zhang, X. Xue, H. Lv, A 28 nm 512 kb adjacent 2t2r rram puf with interleaved cell mirroring and self-adaptive splitting for high density and low ber cryptographic key in iot devices. Microelectron. J. **128**, 105550 (2022)
4. X. Xue, J. Yang, Y. Zhang, M. Wang, H. Lv, X. Zeng, M. Liu, A 28nm 512kb adjacent 2t2r rram puf with interleaved cell mirroring and self-adaptive splitting for extremely low bit error rate

of cryptographic key, in: *2019 IEEE Asian Solid-State Circuits Conference (A-SSCC)*, (IEEE, 2019), pp. 29–32
5. N. Arun, S. Nageswara Rao, A. Pathak, Effects of bottom electrode materials on the resistive switching characteristics of hfo2-based rram devices. J. Elec. Mater. 1–11 (2022)
6. M.J. Marinella, Radiation effects in advanced and emerging non-volatile memories. IEEE Trans. Nucl. Sci. **68**(5), 546–572 (2021)
7. A.P. Patil, C.C. Revadekar, G.U. Kamble, S.S. Kundale, S.J. Kadam, S.S. Sutar, P.J. Patil, T.D. Dongale, Investigations on resistive switching effect and time series statistical analysis of solution combustion synthesized zntio3 memristive device. J. Mater. Sci. Mater. Electron. 1–14 (2022)
8. L. Yin, R. Cheng, Z. Wang, F. Wang, M.G. Sendeku, Y. Wen, X. Zhan, J. He, Two-dimensional unipolar memristors with logic and memory functions. Nano Lett. **20**(6), 4144–4152 (2020)
9. C. Li, M. Hu, Y. Li, H. Jiang, N. Ge, E. Montgomery, J. Zhang, W. Song, N. Dávila, C.E. Graves et al., Analogue signal and image processing with large memristor crossbars. Nat. Electron. **1**(1), 52–59 (2018)
10. Z. Zhou, F. Yang, S. Wang, L. Wang, X. Wang, C. Wang, Y. Xie, Q. Liu, Emerging of two-dimensional materials in novel memristor. Front. Phys. **17**(2), 1–14 (2022)
11. F. Zhou, Z. Zhou, J. Chen, T.H. Choy, J. Wang, N. Zhang, Z. Lin, S. Yu, J. Kang, H.-S.P. Wong et al., Optoelectronic resistive random access memory for neuromorphic vision sensors. Nat. Nanotechnol. **14**(8), 776–782 (2019)
12. F. Liao, F. Zhou, Y. Chai, Neuromorphic vision sensors: Principle, progress and perspectives. J. Semicond. **42**(1), 013105 (2021). https://doi.org/10.1088/1674-4926/42/1/013105
13. K. Lu, X. Li, Q. Sun, X. Pang, J. Chen, T. Minari, X. Liu, Y. Song, Solution-processed electronics for artificial synapses. Mater. Horiz. **8**(2), 447–470 (2021)
14. X. Zhang, A. Huang, Q. Hu, Z. Xiao, P.K. Chu, Neuromorphic computing with memristor crossbar. Phys. Status Solidi (A) **215**(13), 1700875 (2018)
15. G. Bersuker, M. Mason, K.L. Jones, Neuromorphic computing: The potential for high-performance processing in space. Game Changer, 1–12 (2018)
16. J. Bi, B. Li, K. Xi, L. Luo, L. Ji, H. Wang, M. Liu, Total ionization dose and single event effects of a commercial stand-alone 4 mb resistive random access memory (reram). Microelectron. Reliab. **100**, 113443 (2019)
17. H. Zhao, Z. Liu, J. Tang, B. Gao, Q. Qin, J. Li, Y. Zhou, P. Yao, Y. Xi, Y. Lin et al., Energy-efficient high-fidelity image reconstruction with memristor arrays for medical diagnosis. Nat. Commun. **14**(1), 2276 (2023)
18. Y.H. Jang, W. Kim, J. Kim, K.S. Woo, H.J. Lee, J.W. Jeon, S.K. Shim, J. Han, C.S. Hwang, Time-varying data processing with nonvolatile memristor-based temporal kernel. Nat. Commun. **12**(1), 5727 (2021)
19. C.E. Graves, C. Li, X. Sheng, D. Miller, J. Ignowski, L. Kiyama, J.P. Strachan, In-memory computing with memristor content addressable memories for pattern matching. Adv Mater. **32**(37), 2003437 (2020)
20. A.K. Yagati, S.-U. Kim, T. Lee, J. Min, J.-W. Choi, Recombinant azurin-cdse/zns hybrid structures for nanoscale resistive random access memory device. Biosens. Bioelectron. **90**, 23–30 (2017)
21. M. Lanza, A. Sebastian, W.D. Lu, M. Le Gallo, M.-F. Chang, D. Akinwande, F.M. Puglisi, H.N. Alshareef, M. Liu, J.B. Roldan, Memristive technologies for data storage, computation, encryption, and radio-frequency communication. Science **376**(6597), 9979 (2022)
22. E. Onyejegbu, Z. Zhumabay, A. Marzuki, I.A. Ukaegbu, A variable bandwidth memristor-based legendre optimum low pass filter for radio frequency applications. Eng. Rep. **4**(11), 12513 (2022)
23. J.-M. Hung, C.-X. Xue, H.-Y. Kao, Y.-H. Huang, F.-C. Chang, S.-P. Huang, T.-W. Liu, C.-J. Jhang, C.-I. Su, W.-S. Khwa et al., A four-megabit compute-in-memory macro with eight-bit precision based on cmos and resistive random-access memory for ai edge devices. Nat. Electron. **4**(12), 921–930 (2021)
24. F. Zahoor, T.Z.A. Zulkifli, F.A. Khanday, S.A.Z. Murad, Carbon nanotube and resistive random access memory based unbalanced ternary logic gates and basic arithmetic circuits. IEEE Access **8**, 104701–104717 (2020)
25. B.J. Ree, T. Isono, T. Satoh, Chemically controlled volatile and nonvolatile resistive memory characteristics of novel oxygen-based polymers. ACS Appl. Mater. Interfaces **12**(25), 28435–28445 (2020)
26. L. Liu, C. Liu, L. Jiang, J. Li, Y. Ding, S. Wang, Y.-G. Jiang, Y.-B. Sun, J. Wang, S. Chen et al., Ultrafast non-volatile flash memory based on van der waals heterostructures. Nat. Nanotechnol. **16**(8), 874–881 (2021)
27. S.-G. Yi, M.U. Park, S.H. Kim, C.J. Lee, J. Kwon, G.-H. Lee, K.-H. Yoo, Artificial synaptic emulators based on mos2 flash memory devices with double floating gates. ACS Appl. Mater. Interfaces **10**(37), 31480–31487 (2018)
28. P. Gkoupidenis, D.A. Koutsouras, G.G. Malliaras, Neuromorphic device architectures with global connectivity through electrolyte gating. Nat. Commun. **8**(1), 1–8 (2017)
29. L.-G. Wang, Z.-Y. Cao, X. Qian, L. Zhu, D.-P. Cui, A.-D. Li, D. Wu, Atomic layer deposited oxide-based nanocomposite structures with embedded copt x nanocrystals for resistive random access memory applications. ACS Appl. Mater. Interfaces **9**(7), 6634–6643 (2017)
30. J. Shalf, The future of computing beyond moore's law. Phil. Trans. R. Soc. A **378**(2166), 20190061 (2020)
31. T. Li, H. Yu, S.H.Y. Chen, Y. Zhou, S.-T. Han, The strategies of filament control for improving the resistive switching performance. J. Mater. Chem. C **8**(46), 16295–16317 (2020)
32. E. Grimaldi, V. Krizakova, G. Sala, F. Yasin, S. Couet, G. Sankar Kar, K. Garello, P. Gambardella, Single-shot dynamics of spin-orbit torque and spin transfer torque switching in three-terminal magnetic tunnel junctions. Nat. Nanotechnol. **15**(2), 111–117 (2020)
33. T. Eshita, W. Wang, K. Nomura, K. Nakamura, H. Saito, H. Yamaguchi, S. Mihara, Y. Hikosaka, Y. Kataoka, M. Kojima, Development of highly reliable ferroelectric random access memory and its internet of things applications. Jpn. J. Appl. Phys. **57**(11S), 11–01 (2018)
34. T. Mikolajick, S. Slesazeck, M.H. Park, U. Schroeder, Ferroelectric hafnium oxide for ferroelectric random-access memories and ferroelectric field-effect transistors. MRS Bull. **43**(5), 340–346 (2018)
35. K. Ding, J. Wang, Y. Zhou, H. Tian, L. Lu, R. Mazzarello, C. Jia, W. Zhang, F. Rao, E. Ma, Phase-change heterostructure enables ultralow noise and drift for memory operation. Science. **366**(6462), 210–215 (2019)
36. J. Meng, Y. Gui, B.M. Nouri, G. Comanescu, X. Ma, Y. Zhang, C.-C. Popescu, M. Kang, M. Miscuglio, N. Peserico et al., Electrical programmable multi-level non-volatile photonic random-access memory. arXiv preprint arXiv:2203.13337 (2022)
37. H. Kim, J.S. Han, S.G. Kim, S.Y. Kim, H.W. Jang, Halide perovskites for resistive random-access memories. J. Mater. Chem. C. **7**(18), 5226–5234 (2019)
38. M. Seal, A. Deogaonkar, A. Senapati, S. Maikap, N. Raghavan, Ruthenium based rram for low variability switching and scaling for contemporary computing systems. Microelectron. Reliab. **114623** (2022)
39. H.-H. Choi, S.H. Paik, Y. Kim, M. Kim, Y.S. Kang, S.-S. Lee, J.Y. Jho, J.H. Park, Facilitation of the thermochemical mechanism in

nio-based resistive switching memories via tip-enhanced electric fields. J. Ind. Eng. Chem. **94**, 233–239 (2021)
40. W.-K. Hsieh, R.W. Chuang, S.-J. Chang, Two-bit-per-cell resistive switching memory device with a ti/mgzno/pt structure. RSC Adv. **5**(107), 88166–88170 (2015)
41. W. Wan, R. Kubendran, C. Schaefer, S.B. Eryilmaz, W. Zhang, D. Wu, S. Deiss, P. Raina, H. Qian, B. Gao et al., A compute-in-memory chip based on resistive random-access memory. Nature **608**(7923), 504–512 (2022)
42. L. Yan, L. Ruan, F. Luo, J. Tong, C. Sun, Y. Zheng, X. Han, Y. Zhang, X. Zhang, Enhanced resistive switching behavior of ch3nh3pbi3 based resistive random access memory by nickel doping. Vacuum **198**, 110862 (2022)
43. D.B. Strukov, G.S. Snider, D.R. Stewart, S. Williams, Memristor: The fourth fundamental passive circuit element. HP TechCon. **2008**, 1–3 (2008)
44. K. Liu, L. Qin, X. Zhang, J. Zhu, X. Sun, K. Yang, Y. Cai, Y. Yang, R. Huang, Interfacial redox processes in memristive devices based on valence change and electrochemical metallization. Faraday Discuss. **213**, 41–52 (2019)
45. A. Regoutz, I. Gupta, A. Serb, A. Khiat, F. Borgatti, T.-L. Lee, C. Schlueter, P. Torelli, B. Gobaut, M. Light et al., Role and optimization of the active oxide layer in tio2-based rram. Adv. Funct. Mater. **26**(4), 507–513 (2016)
46. G. Ding, Y. Wang, G. Zhang, K. Zhou, K. Zeng, Z. Li, Y. Zhou, C. Zhang, X. Chen, S.-T. Han, 2d metal-organic framework nanosheets with time-dependent and multilevel memristive switching. Adv. Funct. Mater. **29**(3), 1806637 (2019)
47. S. Sarkar, H. Banik, S. Suklabaidya, B. Deb, S. Majumdar, P.K. Paul, D. Bhattacharjee, S.A. Hussain, Resistive switching of the tetraindolyl derivative in ultrathin films: A potential candidate for nonvolatile memory applications. Langmuir **37**(15), 4449–4459 (2021)
48. W.-Y. Huang, Y.-C. Chang, Y.-F. Sie, C.-R. Yu, C.-Y. Wu, Y.-L. Hsu, Bio-cellulose substrate for fabricating fully biodegradable resistive random access devices. ACS Appl. Polym. Mater. **3**(9), 4478–4484 (2021)
49. D. Liu, Q. Lin, Z. Zang, M. Wang, P. Wangyang, X. Tang, M. Zhou, W. Hu, Flexible all-inorganic perovskite cspbbr3 nonvolatile memory device. ACS Appl. Mater. Interfaces **9**(7), 6171–6176 (2017)
50. C. Cuhadar, S.-G. Kim, J.-M. Yang, J.-Y. Seo, D. Lee, N.-G. Park, All-inorganic bismuth halide perovskite-like materials a3bi2i9 and a3bi1 8na0 2i8 6 (a= rb and cs) for low-voltage switching resistive memory. ACS Appl. Mater. Interfaces **10**(35), 29741–29749 (2018)
51. X. Cao, Y. Han, J. Zhou, W. Zuo, X. Gao, L. Han, X. Pang, L. Zhang, Y. Liu, S. Cao, Enhanced switching ratio and long-term stability of flexible rram by anchoring polyvinylammonium on perovskite grains. ACS Appl. Mater. Interfaces **11**(39), 35914–35923 (2019)
52. C. Gu, J.-S. Lee, Flexible hybrid organic-inorganic perovskite memory. ACS Nano **10**(5), 5413–5418 (2016)
53. B. Guo, B. Sun, W. Hou, Y. Chen, S. Zhu, S. Mao, L. Zheng, M. Lei, B. Li, G. Fu, A sustainable resistive switching memory device based on organic keratin extracted from hair. RSC Adv. **9**(22), 12436–12440 (2019)
54. L. Zhang, B. Xie, W. Chen, L. Fan, H. Zheng, Q. Wu, P. Zheng, L. Zheng, Y. Zhang, Resistive switching behaviours of pt/ni0. 5zn0. 5fe2o4/pt based on film thickness for memristor applications. Ceram. Int. (2022)
55. J. Li, C. Yao, Y. Ke, W. Huang, S.K. Thatikonda, N. Qin, D. Bao, Understanding the coexistence of unipolar and bipolar resistive switching in nife2o4 resistive memory devices. Appl. Phys. Lett. **120**(13), 133501 (2022)
56. M.E. Hajlaoui, E. Dhahri, K. Khirouni, High resistance and giant permittivity study of ni0. 4zn0. 6fe2o4 spinel ferrite as a function of frequency and temperature. J. Mater. Sci. Mat. Electron. **33**(23), 18858–18870 (2022)
57. M. Nasri, C. Henchiri, R. Dhahri, J. Khelifi, H. Rahmouni, E. Dhahri, L. Omari, A. Tozri, M.R. Berber, Structural, dielectric, electrical and modulus spectroscopic characteristics of cofecuo4 spinel ferrite nanoparticles. Mater. Sci. Eng. B **272**, 115331 (2021)
58. S.B. Kale, S.B. Somvanshi, M. Sarnaik, S. More, S. Shukla, K. Jadhav, Enhancement in surface area and magnetization of cofe2o4 nanoparticles for targeted drug delivery application, in: *AIP Conference Proceedings*, vol. 1953, (AIP Publishing LLC, 2018), pp. 030193
59. M.M.L. Sonia, S. Anand, V.M. Vinosel, M.A. Janifer, S. Pauline, A. Manikandan, Effect of lattice strain on structure, morphology and magneto-dielectric properties of spinel nigdxfe2- xo4 ferrite nano-crystallites synthesized by sol-gel route. J. Magn. Magn. Mater. **466**, 238–251 (2018)
60. V.K. Chakradhary, A. Ansari, M.J. Akhtar, Design, synthesis, and testing of high coercivity cobalt doped nickel ferrite nanoparticles for magnetic applications. J. Magn. Magn. Mater. **469**, 674–680 (2019)
61. N. Adeela, U. Khan, S. Naz, K. Khan, R. Sagar, S. Aslam, D. Wu, Role of ni concentration on structural and magnetic properties of inverse spinel ferrite. Mater. Res. Bull. **107**, 60–65 (2018)
62. M.C. Mathpal, G. Niraula, M. Chand, P. Kumar, M.K. Singh, S.K. Sharma, M.A. Soler, H. Swart, State of art of spinel ferrites enabled humidity sensors. Spinel Nanoferrites, 437–475 (2021)
63. H.H. Kora, M. Taha, A. Abdelwahab, A.A. Farghali, S. El-Dek, Effect of pressure on the geometric, electronic structure, elastic, and optical properties of the normal spinel mgfe2o4: a first-principles study. Mater. Res. Express **7**(10), 106101 (2020)
64. S.B. Narang, K. Pubby, Nickel spinel ferrites: a review. J. Magn. Magn. Mater. **519**, 167163 (2021)
65. S. Madake, M. Hattali, K. Rajpure, Porogen induced formation of mesoporous zinc ferrite thin films and their chemiresistive properties. Mater. Sci. Eng. B **263**, 114867 (2021)
66. S. Nikam, A. Sharma, M. Rahaman, A. Teli, S. Mujawar, D. Zahn, P. Patil, S. Sahoo, G. Salvan, P. Patil, Pulsed laser deposited cofe 2 o 4 thin films as supercapacitor electrodes. RSC Adv. **10**(33), 19353–19359 (2020)
67. M. Almessiere, A.D. Korkmaz, Y. Slimani, M. Nawaz, S. Ali, A. Baykal, Magneto-optical properties of rare earth metals substituted co-zn spinel nanoferrites. Ceram. Int. **45**(3), 3449–3458 (2019)
68. A.G. Abraham, A. Manikandan, E. Manikandan, S. Vadivel, S. Jaganathan, A. Baykal, P.S. Renganathan, Enhanced magneto-optical and photo-catalytic properties of transition metal cobalt (co2+ ions) doped spinel mgfe2o4 ferrite nanocomposites. J. Magn. Magn. Mater. **452**, 380–388 (2018)
69. A. Kumar, J. Shen, W. Yang, H. Zhao, P. Sharma, D. Varshney, Q. Li, Impact of rare earth gd3+ ions on structural and magnetic properties of ni0. 5zn0. 5fe2- x gd x o4 spinel ferrite: Useful for advanced spintronic technologies. J. Supercond. Nov. Magn. **31**(4), 1173–1182 (2018)
70. S. Emori, P. Li, Ferrimagnetic insulators for spintronics: Beyond garnets. J. Appl. Phys. **129**(2), 020901 (2021)
71. S. Mallesh, V. Srinivas, A comprehensive study on thermal stability and magnetic properties of mnzn-ferrite nanoparticles. J. Magn. Magn. Mater. **475**, 290–303 (2019)
72. S.B. Somvanshi, M.V. Khedkar, P.B. Kharat, K. Jadhav, Influential diamagnetic magnesium (mg2+) ion substitution in nano-spinel zinc ferrite (znfe2o4): thermal, structural, spectral, optical and physisorption analysis. Ceram. Int. **46**(7), 8640–8650 (2020)

73. J.-H. Cho, Y.J. Kim, S.H. Kim, Y.-J. Lee, J.-Y. Choi, G.-T. Hwang, J. Ryu, S.K. Kwak, W. Jo, Modulation of magnetoelectric coupling through systematically engineered spin canting in nickel-zinc ferrite. J. Am. Ceram. Soc. **105**(4), 2655–2662 (2022)
74. M. Umair, A. Quader, M. Imran, M.A. Yaqub, S.M. Ramay, S. Atiq, Significant impact of spinel ferrites in evolution of magneto-electric coupling in novel tri-phase composites. Ceram. Int. **48**(10), 14473–14480 (2022)
75. T. Dongale, A. Bagade, S. Mohite, A. Rananavare, M. Orlowski, R. Kamat, K. Rajpure, Bipolar resistive switching with coexistence of mem-elements in the spray deposited cofe2o4 thin film. J. Mater. Sci. Mater. Electron. **29**(4), 3231–3238 (2018)
76. T.D. Dongale, S.S. Khot, A.A. Patil, S.V. Wagh, P.B. Patil, D.P. Dubal, T.G. Kim, Bifunctional nanoparticulated nickel ferrite thin films: Resistive memory and aqueous battery applications. Mater. Des. **201**, 109493 (2021)
77. K. Gayakvad, K. Patankar, Cobalt ferrite as an active material for resistive random-access memory. Pramana **95**(4), 1–6 (2021)
78. M. Kamran, M. Anis-ur-Rehman, Resistive switching effect in re-doped cobalt ferrite nanoparticles. Ceram. Int. **48**(12), 16912–16922 (2022)
79. C. Jin, E. Jiang, H. Bai, Resistive hysteresis and capacitance effect in nife2o4/srtio3: Nb (1 wt%) junctions. Appl. Surf. Sci. **257**(21), 8998–9001 (2011)
80. W. Hu, N. Qin, G. Wu, Y. Lin, S. Li, D. Bao, Opportunity of spinel ferrite materials in nonvolatile memory device applications based on their resistive switching performances. J. Am. Chem. Soc. **134**(36), 14658–14661 (2012)
81. W. Hu, X. Chen, G. Wu, Y. Lin, N. Qin, D. Bao, Bipolar and tri-state unipolar resistive switching behaviors in ag/znfe2o4/pt memory devices. Appl. Phys. Lett. **101**(6), 063501 (2012)
82. C. Jiang, L. Wu, W. Wei, C. Dong, J. Yao, The resistive switching memory of cofe2o4 thin film using nanoporous alumina template. Nanoscale Res. Lett. **9**(1), 1–5 (2014)
83. W. Hu, L. Zou, R. Chen, W. Xie, X. Chen, N. Qin, S. Li, G. Yang, D. Bao, Resistive switching properties and physical mechanism of cobalt ferrite thin films. Appl. Phys. Lett. **104**(14), 143502 (2014)
84. Q. Wang, Y. Zhu, X. Liu, M. Zhao, M. Wei, F. Zhang, Y. Zhang, B. Sun, M. Li, Study of resistive switching and magnetism modulation in the pt/cofe2o4/nb: Srtio3 heterostructures. Appl. Phys. Lett. **107**(6), 063502 (2015)
85. M. Mustaqima, P. Yoo, W. Huang, B.W. Lee, C. Liu, Regulation of the forming process and the set voltage distribution of unipolar resistance switching in spin-coated cofe2o4 thin films. Nanoscale Res. Lett. **10**(1), 1–7 (2015)
86. Z. Xiahou, D.H. Kim, H. Xu, Y. Li, B.W. Lee, C. Liu, Cu doping effect on the resistive switching behaviors of cofe2o4 thin films. J. Mater. Sci. Mater. Electron. **27**(3), 2255–2259 (2016)
87. G. Gong, C. Wu, P. Hu, Y. Li, N. Kwon, C. Liu, Thickness effect on the stability of unipolar resistance switching in tin ferrite thin films. Curr. Appl. Phys. **16**(9), 980–984 (2016)
88. B. Sun, X. Zhang, G. Zhou, C. Zhang, P. Li, Y. Xia, Y. Zhao, Effect of Cu ions assisted conductive filament on resistive switching memory behaviors in znfe2o4-based devices. J. Alloys Compd. **694**, 464–470 (2017)
89. P. Ghosh, R. Bhowmik, M. Das, P. Mitra, Electrical conductivity and magnetic field dependent current-voltage characteristics of nanocrystalline nickel ferrite. Phys. E: Low-Dimens. Syst. Nanostructures. **88**, 218–227 (2017)
90. Q. Wang, Y. Zhu, X. Liu, M. Zhao, M. Wei, F. Zhang, Y. Zhang, M. Li, M. Li, Electric field modulation of resistive switching and related magnetism in the pt/nife2o4/nb: Srtio3 heterostructures. J. Alloys Compd. **693**, 945–949 (2017)
91. A. Hao, S. He, N. Qin, R. Chen, D. Bao, Ce-doping induced enhancement of resistive switching performance of pt/nife2o4/pt memory devices. Ceram. Int. **43**, 481–487 (2017)
92. A. Hao, M. Ismail, S. He, N. Qin, W. Huang, J. Wu, D. Bao, Ag-nps doping enhanced resistive switching performance and induced changes in magnetic properties of nife 2 o 4 thin films. RSC Adv. **7**(74), 46665–46677 (2017)
93. S. Munjal, N. Khare, Valence change bipolar resistive switching accompanied with magnetization switching in cofe2o4 thin film. Sci. Rep. **7**(1), 1–10 (2017)
94. O.S. Bagal, S.S. Bhosale, A.A. Bagade, K.Y. Rajpure, R.K. Kamat, T.D. Dongale, Development of ag/cofe2o4/fto thin film memristive device using spray pyrolysis method
95. A. Hao, M. Ismail, S. He, N. Qin, R. Chen, A.M. Rana, D. Bao, Enhanced resistive switching and magnetic properties of gd-doped nife2o4 thin films prepared by chemical solution deposition method. Mater. Sci. Eng. B **229**, 86–95 (2018)
96. A. Hao, M. Ismail, S. He, N. Qin, W. Huang, J. Wu, D. Bao, Improved unipolar resistive switching characteristics of au-doped nickel ferrite magnetic thin films for nonvolatile memory applications. J. Alloys Compd. **732**, 573–584 (2018)
97. A. Hao, M. Ismail, S. He, W. Huang, N. Qin, D. Bao, Coexistence of unipolar and bipolar resistive switching behaviors in nife2o4 thin film devices by doping ag nanoparticles. J. Appl. Phys. **123**(8), 085108 (2018)
98. M. Ismail, A. Hao, W. Huang, J. Lee, S. Kim, D. Bao, Coexistence of unipolar and bipolar switching in nanocrystalline spinel ferrite znfe2o4 thin films synthesized by sol-gel method. Appl. Phys. Lett. **113**(15), 152103 (2018)
99. M. Ismail, A. Hao, S. He, W. Huang, N. Qin, D. Bao, Reversible transitions among four modes of nonpolar resistive switching characteristics in nano-crystalline zinc ferrite magnetic thin films. J. Alloys Compd. **753**, 100–110 (2018)
100. S. Munjal, N. Khare, Multilevel resistive and magnetization switching in cu/cofe2o4/pt device: Coexistence of ionic and metallic conducting filaments. Appl. Phys. Lett. **113**(24), 243501 (2018)
101. A. Hao, D. Jia, M. Ismail, W. Huang, R. Chen, D. Bao, Electric field induced manipulation of resistive and magnetization switching in pt/nife1. 95cr0. 05o4/pt memory devices. Appl. Phys. Lett. **114**(20), 203502 (2019)
102. L. Wu, C. Dong, X. Wang, J. Li, M. Li, Annealing effect on the bipolar resistive switching memory of nizn ferrite films. J. Alloys Compd. **779**, 794–799 (2019)
103. A. Hao, D. Jia, M. Ismail, R. Chen, D. Bao, Controlling of resistive switching and magnetism through cu2+ ions substitution in nickel ferrite based nonvolatile memory. J. Alloys Compd. **790**, 70–77 (2019)
104. S. Munjal, N. Khare, Forming free resistive switching characteristics in al/nife2o4/fto device, in: *AIP Conference Proceedings*, vol. 2220, (AIP Publishing LLC, 2020) pp. 020171
105. S. Munjal, N. Khare, Compliance current controlled volatile and nonvolatile memory in ag/cofe2o4/pt resistive switching device. Nanotechnology. **32**(18), 185204 (2021)
106. J. Li, C. Yao, W. Huang, N. Qin, D. Bao, Highly uniform resistive switching properties of nife2o4 films by embedding well-ordered pyramid-shaped pt/au nanostructures. J. Alloys Compd. **890**, 161814 (2022)
107. S.-K. Tong, J.-H. Chang, Y.-H. Hao, M.-R. Wu, D.-H. Wei, Y.-L. Chueh, Optimum resistive switching characteristics of nife2o4 by controlling film thickness. Appl. Surf. Sci. **564**, 150091 (2021)
108. S. Rajarathinam, U. Ganguly, N. Venkataramani, Impact of oxygen partial pressure on resistive switching characteristics of pld deposited znfe2o4 thin films for rram devices. Ceram. Int. **48**(6), 7876–7884 (2022)
109. S. Wang, X. Ning, A. Hao, R. Chen, Metal nanoparticles layer boosted resistive switching property in nife2o4-based memory devices. J. Alloys Compd. **908**, 164569 (2022)

110. M. Kumara, W. Clower, K. Seetala, J.B. Joffrion, C.G. Wilson, Resistive switching of transition metal ferrites on silicon substrate. Mater. Lett. **309**, 131467 (2022)
111. D.B. Strukov, G.S. Snider, D.R. Stewart, R.S. Williams, The missing memristor found. Nature **453**(7191), 80–83 (2008)
112. B.D. Hoskins, G.C. Adam, E. Strelcov, N. Zhitenev, A. Kolmakov, D.B. Strukov, J.J. McClelland, Stateful characterization of resistive switching tio2 with electron beam induced currents. Nat. Commun. **8**(1), 1–11 (2017)
113. L. Chua, Memristor-the missing circuit element. IEEE Trans. Circ Theory **18**(5), 507–519 (1971)
114. K.M. Sundqvist, D.K. Ferry, L.B. Kish, Memristor equations: Incomplete physics and undefined passivity/activity. Fluct. Noise Lett. **16**(04), 1771001 (2017)
115. K.-J. Lee, L.-W. Wang, T.-K. Chiang, Y.-H. Wang, Effects of electrodes on the switching behavior of strontium titanate nickelate resistive random access memory. Materials **8**(10), 7191–7198 (2015)
116. R. Zhang, K.-C. Chang, T.-C. Chang, T.-M. Tsai, S.-Y. Huang, W.-J. Chen, K.-H. Chen, J.-C. Lou, J.-H. Chen, T.-F. Young et al., Characterization of oxygen accumulation in indium-tin-oxide for resistance random access memory. IEEE Electron Device Lett. **35**(6), 630–632 (2014)
117. D.P. Sahu, S.N. Jammalamadaka, Remote control of resistive switching in tio2 based resistive random access memory device. Sci. Rep. **7**(1), 17224 (2017)
118. G. Zhou, L. Xiao, S. Zhang, B. Wu, X. Liu, A. Zhou, Mechanism for an enhanced resistive switching effect of bilayer niox/tio2 for resistive random access memory. J. Alloys Compd. **722**, 753–759 (2017)
119. S. Ren, G. Zhu, J. Xie, J. Bu, H. Qin, J. Hu, Resistive switching and electrical control of ferromagnetism in a ag/hfo2/nb: Srtio3/ag resistive random access memory (rram) device at room temperature. J. Phys. Condens. Matter **28**(5), 056001 (2016)
120. Y. Yang, M. Wu, X. Li, H. Hu, Z. Jiang, Z. Li, X. Hao, C. Zheng, X. Lou, S.J. Pennycook et al., The role of ferroelectric polarization in resistive memory properties of metal/insulator/semiconductor tunnel junctions: a comparative study. ACS Appl. Mater. Interfaces **12**(29), 32935–32942 (2020)
121. R. Meyer, J.R. Contreras, A. Petraru, H. Kohlstedt, On a novel ferro resistive random access memory (frram): Basic model and first experiments. Integr. Ferroelectr. **64**(1), 77–88 (2004)
122. H. Akinaga, H. Shima, Resistive random access memory (reram) based on metal oxides. Proc. IEEE **98**(12), 2237–2251 (2010)
123. Y. Zhang, M. Liu, C. Ma, L. Lu, C.Y. Han, Electrochemically driven dual bipolar resistive switching in lanio 3/smnio 3/nb: Srtio 3 heterostructures fabricated through selective area epitaxy. J. Mater. Chem. C **10**(19), 7707–7716 (2022)
124. N. Pandya, A. Debnath, U. Joshi, Resistance switching and memory effects in solution-processed bifeo3/lanio3 junctions. J. Phys. D Appl. Phys. **49**(5), 055301 (2015)
125. S. Ghosh, D. Basak, Light-assisted resistive switching memory device with reduced set/reset voltage using sol-gel tio2 on al-doped zno electrode. Phys Status Solidi (A) **218**(14), 2100112 (2021)
126. F.M. Simanjuntak, D. Panda, T.-L. Tsai, C.-A. Lin, K.-H. Wei, T.-Y. Tseng, Enhancing the memory window of azo/zno/ito transparent resistive switching devices by modulating the oxygen vacancy concentration of the top electrode. J. Mater. Sci. **50**, 6961–6969 (2015)
127. K. Zheng, X. Sun, J. Zhao, Y. Wang, H. Yu, H.V. Demir, K. Teo, An indium-free transparent resistive switching random access memory. IEEE Electron Device Lett. **32**(6), 797–799 (2011)
128. K. Kinoshita, T. Okutani, H. Tanaka, T. Hinoki, H. Agura, K. Yazawa, K. Ohmi, S. Kishida, Flexible and transparent reram with gzo memory layer and gzo-electrodes on large pen sheet. Solid State Electron. **58**(1), 48–53 (2011)
129. C. Hao, F. Wen, J. Xiang, S. Yuan, B. Yang, L. Li, W. Wang, Z. Zeng, L. Wang, Z. Liu et al., Liquid-exfoliated black phosphorous nanosheet thin films for flexible resistive random access memory applications. Adv. Funct. Mater. **26**(12), 2016–2024 (2016)
130. J.H. Lee, S.P. Park, K. Park, H.J. Kim, Flexible and waterproof resistive random-access memory based on nitrocellulose for skin-attachable wearable devices. Adv. Funct. Mater. **30**(1), 1907437 (2020)
131. Y. Huang, Z. Shen, Y. Wu, X. Wang, S. Zhang, X. Shi, H. Zeng, Amorphous zno based resistive random access memory. RSC Adv. **6**(22), 17867–17872 (2016)
132. J. Di, J. Du, Z. Lin, S. Liu, J. Ouyang, J. Chang, Recent advances in resistive random access memory based on lead halide perovskite. InfoMat **3**(3), 293–315 (2021)
133. Y. Li, S. Long, Q. Liu, H. Lü, S. Liu, M. Liu, An overview of resistive random access memory devices. Chin. Sci. Bull. **56**, 3072–3078 (2011)
134. M. Yi, Y. Cao, H. Ling, Z. Du, L. Wang, T. Yang, Q. Fan, L. Xie, W. Huang, Temperature dependence of resistive switching behaviors in resistive random access memory based on graphene oxide film. Nanotechnology **25**(18), 185202 (2014)
135. H. Tian, H.-Y. Chen, T.-L. Ren, C. Li, Q.-T. Xue, M.A. Mohammad, C. Wu, Y. Yang, H.-S.P. Wong, Cost-effective, transfer-free, flexible resistive random access memory using laser-scribed reduced graphene oxide patterning technology. Nano Lett. **14**(6), 3214–3219 (2014)
136. Q. Luo, X. Zhang, Y. Hu, T. Gong, X. Xu, P. Yuan, H. Ma, D. Dong, H. Lv, S. Long et al., Self-rectifying and forming-free resistive-switching device for embedded memory application. IEEE Electron Device Lett. **39**(5), 664–667 (2018)
137. Q. Wu, W. Banerjee, J. Cao, Z. Ji, L. Li, M. Liu, Improvement of durability and switching speed by incorporating nanocrystals in the hfox based resistive random access memory devices. Appl. Phys. Lett. **113**(2), 023105 (2018)
138. D. Acharyya, A. Hazra, P. Bhattacharyya, A journey towards reliability improvement of tio2 based resistive random access memory: a review. Microelectron. Reliab. **54**(3), 541–560 (2014)
139. J. Zhao, Y. Li, J. Li, L. Zhou, Role and optimization of thermal rapid annealing in ta/taox/ru based resistive switching memory. Vacuum **191**, 110392 (2021)
140. J.W. Seo, S.J. Baik, S.J. Kang, K.S. Lim, Characteristics of zno thin film for the resistive random access memory. MRS Online Proc. Library (OPL). **1250** (2010)
141. W.-Y. Chang, H.-W. Huang, W.-T. Wang, C.-H. Hou, Y.-L. Chueh, J.-H. He, High uniformity of resistive switching characteristics in a cr/zno/pt device. J. Electrochem. Soc. **159**(3), 29 (2012)
142. J. Jeong, M.J. Kim, W.S. Hwang, B.J. Cho, Copolymer-based flexible resistive random access memory prepared by initiated chemical vapor deposition process. Adv. Electron. Mater. **7**(10), 2100375 (2021)
143. K.-L. Lin, T.-H. Hou, Y.-J. Lee, J.-W. Chang, J.-H. Lin, J. Shieh, C.-T. Chou, T.-F. Lei, W.-H. Chang, W.-Y. Jang et al., Switching mode and mechanism in binary oxide resistive random access memory using ni electrode. Jpn. J. Appl. Phys. **52**(3R), 031801 (2013)
144. Y. Li, L. Yin, Z. Wu, X. Li, X. Song, X. Gao, L. Fu, Improved resistive switching uniformity of sio 2 electrolyte-based resistive random access memory device with cu oxidizable electrode. IEEE Electron Device Lett. **40**(10), 1599–1601 (2019)
145. T. Nagata, M. Haemori, Y. Yamashita, H. Yoshikawa, Y. Iwashita, K. Kobayashi, T. Chikyow, Bias application hard x-ray photoelectron spectroscopy study of forming process of cu/hfo2/pt resistive random access memory structure. Appl. Phys. Lett. **99**(22), 223517 (2011)

146. M. Ismail, C.-Y. Huang, D. Panda, C.-J. Hung, T.-L. Tsai, J.-H. Jieng, C.-A. Lin, U. Chand, A.M. Rana, E. Ahmed et al., Forming-free bipolar resistive switching in nonstoichiometric ceria films. Nanoscale Res. Lett. **9**, 1–8 (2014)
147. F. Hui, E. Grustan-Gutierrez, S. Long, Q. Liu, A.K. Ott, A.C. Ferrari, M. Lanza, Graphene and related materials for resistive random access memories. Adv. Electron. Mater. **3**(8), 1600195 (2017)
148. Y. Ahn, H.W. Shin, T.H. Lee, W.-H. Kim, J.Y. Son, Effects of a nb nanopin electrode on the resistive random-access memory switching characteristics of nio thin films. Nanoscale **10**(28), 13443–13448 (2018)
149. X.-J. Zhu, J. Shang, R.-W. Li, Resistive switching effects in oxide sandwiched structures. Front. Mater. Sci. **6**, 183–206 (2012)
150. Y. Chen, Y. Yan, J. Wu, C. Wang, J.Y. Lin, J.S. Zhao, C.S. Hwang, Electroforming-free, flexible, and reliable resistive random-access memory based on an ultrathin tao x film. ACS Appl. Mater. Interfaces **12**(9), 10681–10688 (2020)
151. Z. Yang, J. Wu, P. Li, Y. Chen, Y. Yan, B. Zhu, C.S. Hwang, W. Mi, J. Zhao, K. Zhang et al., Resistive random access memory based on gallium oxide thin films for self-powered pressure sensor systems. Ceram. Int. **46**(13), 21141–21148 (2020)
152. H.-D. Kim, M. Yun, S. Kim, Self-rectifying resistive switching behavior observed in si3n4-based resistive random access memory devices. J. Alloys Compd. **651**, 340–343 (2015)
153. W. Li, Y. Tuo, W. Mi, D. Wang, M. Wang, L. Zhou, J. Zhao, The effect of oxygen affinity electrode Ti on the performance of vanadium oxide-based valence change resistive random access memory. Vacuum **209**, 111794 (2023)
154. J.B. Roldán, G. González-Cordero, R. Picos, E. Miranda, F. Palumbo, F. Jiménez-Molinos, E. Moreno, D. Maldonado, S.B. Baldomá, M. Moner Al Chawa et al., On the thermal models for resistive random access memory circuit simulation. Nanomaterials **11**(5), 1261 (2021)
155. E. Nowak, E. Chłopocka, M. Szybowicz, Zno and zno-based materials as active layer in resistive random-access memory (rram). Crystals **13**(3), 416 (2023)
156. T. Zhang, Z. Song, F. Rao, G. Feng, B. Liu, S. Feng, B. Chen, High speed chalcogenide random access memory based on si2sb2te5. Jpn. J. Appl. Phys. **46**(3L), 247 (2007)
157. S.P. Park, Y.J. Tak, H.J. Kim, J.H. Lee, H. Yoo, H.J. Kim, Analysis of the bipolar resistive switching behavior of a biocompatible glucose film for resistive random access memory. Adv. Mater. **30**(26), 1800722 (2018)
158. A. Prakash, D. Jana, S. Samanta, S. Maikap, Self-compliance-improved resistive switching using ir/tao x/w cross-point memory. Nanoscale Res. Lett. **8**, 1–6 (2013)
159. T. Ninomiya, K. Katayama, S. Muraoka, R. Yasuhara, T. Mikawa, Z. Wei, Conductive filament expansion in taox bipolar resistive random access memory during pulse cycling. Jpn. J. Appl. Phys. **52**(11R), 114201 (2013)
160. Q. Liu, S. Long, Q. Wang, M. Liu, S. Zhang, J. Chen, Bistable resistance switching of cu/ti: Zro2/pt for nonvolatile memory application. ECS Trans. **18**(1), 49 (2009)
161. W. Banerjee, H. Hwang, Evolution of 0.7 conductance anomaly in electric field driven ferromagnetic cuo junction based resistive random access memory devices. Appl. Phys. Lett. **116**(5), 053502 (2020)
162. J.-C. Wang, D.-Y. Jian, Y.-R. Ye, L.-C. Chang, C.-S. Lai, Characteristics of gadolinium oxide resistive switching memory with pt-al alloy top electrode and post-metallization annealing. J. Phys. D Appl. Phys. **46**(27), 275103 (2013)
163. H. Park, S. Go, C. Lee, H. Nam, J.-K. Lee, J. Lee, Consecutive and selective chemical vapor deposition of pt/al bilayer electrodes for tio2 resistive switching memory. Jpn. J. Appl. Phys. **52**(10S), 10–08 (2013)
164. D.W. Kim, K.-C. Kwon, M.-J. Song, K.-H. Kwon, H.-J. KiM, S.-M. Jin, Y.-J. Son, J.-G. Park, Multi level operation of cuo based cbram with cute electrode, in: *Electrochemical Society Meeting Abstracts*, vol. 228, (The Electrochemical Society, Inc., 2015) pp. 768–768
165. L. Goux, K. Opsomer, R. Degraeve, R. Müller, C. Detavernier, D. Wouters, M. Jurczak, L. Altimime, J. Kittl, Influence of the cu-te composition and microstructure on the resistive switching of cu-te/al2o3/si cells. Appl. Phys. Lett. **99**(5), 053502 (2011)
166. C.-L. Tsai, F. Xiong, E. Pop, M. Shim, Resistive random access memory enabled by carbon nanotube crossbar electrodes. Acs Nano. **7**(6), 5360–5366 (2013)
167. E.C. Ahn, H.-S.P. Wong, E. Pop, Carbon nanomaterials for non-volatile memories. Nat. Rev. Mater. **3**(3), 1–15 (2018)
168. J.Y. Son, Y.-H. Shin, H. Kim, H.M. Jang, Nio resistive random access memory nanocapacitor array on graphene. Acs Nano **4**(5), 2655–2658 (2010)
169. H. Zhao, H. Tu, F. Wei, J. Du, Highly transparent dysprosium oxide-based rram with multilayer graphene electrode for low-power nonvolatile memory application. IEEE Trans. Electron Devices. **61**(5), 1388–1393 (2014)
170. T. Diokh, E. Le-Roux, S. Jeannot, C. Cagli, V. Jousseaume, J.-F. Nodin, M. Gros-Jean, C. Gaumer, M. Mellier, J. Cluzel et al., Study of resistive random access memory based on tin/taox/tin integrated into a 65 nm advanced complementary metal oxide semiconductor technology. Thin Solid Films **533**, 24–28 (2013)
171. S. Petzold, E. Miranda, S. Sharath, J. Muñoz-Gorriz, T. Vogel, E. Piros, N. Kaiser, R. Eilhardt, A. Zintler, L. Molina-Luna et al., Analysis and simulation of the multiple resistive switching modes occurring in hfo x-based resistive random access memories using memdiodes. J. Appl. Phys. **125**(23), 234503 (2019)
172. P. Singh, C.G. Li, P. Pitchappa, C. Lee, Tantalum-nitride antifuse electromechanical otp for embedded memory applications. IEEE Electron Device Lett. **34**(8), 987–989 (2013)
173. S. Jou, B.-R. Hwang, C.-J. Li, Resistance switching properties in cu/cu-sio2/tan device, in: *Proceeding World Congress on Engineering*, vol. 2, (2011), pp. 4
174. R. Prakash, S. Sharma, A. Kumar, D. Kaur, Improved resistive switching performance in cu-cation migrated mos2 based reram device incorporated with tungsten nitride bottom electrode. Curr. Appl. Phys. **19**(3), 260–265 (2019)
175. W.G. Kim, M.G. Sung, S.J. Kim, J.H. Yoo, J.W. Oh, J.N. Kim, B.G. Gyun, T.W. Kim, C.H. Kim, J.Y. Byun et al., Dependence of the switching characteristics of resistance random access memory on the type of transition metal oxide; tio2, zro2, and hfo2. J. Electrochem. Soc. **158**(4), 417 (2011)
176. A. Mehonic, M. Buckwell, L. Montesi, L. Garnett, S. Hudziak, S. Fearn, R. Chater, D. McPhail, A.J. Kenyon, Structural changes and conductance thresholds in metal-free intrinsic siox resistive random access memory. J. Appl. Phys. **117**(12), 124505 (2015)
177. T.J. Yen, A. Gismatulin, V. Volodin, V. Gritsenko, A. Chin, All nonmetal resistive random access memory. Sci. Rep. **9**(1), 6144 (2019)
178. T. Sadi, L. Wang, L. Gerrer, A. Asenov, Physical simulation of si-based resistive random-access memory devices, in: *2015 International Conference on Simulation of Semiconductor Processes and Devices (SISPAD)*, (IEEE, 2015), pp. 385–388
179. C. Lu, J. Yu, X.-W. Chi, G.-Y. Lin, X.-L. Lan, W. Huang, J.-Y. Wang, J.-F. Xu, C. Wang, C. Li et al., Self-compliance pt/hfo2/ti/si one-diode-one-resistor resistive random access memory device and its low temperature characteristics. Appl. Phys. Express **9**(4), 041501 (2016)

180. H.J. Yun, B.J. Choi, Effects of moisture and electrode material on aln-based resistive random access memory. Ceram. Int. **45**(13), 16311–16316 (2019)
181. M. Al-Mamun, A. Chakraborty, M. Orlowski, Analysis of the electrical reram device degradation induced by thermal cross-talk. Adv. Electron. Mater. **9**(4), 2201081 (2023)
182. W. Xiao, W. Song, Y.P. Feng, D. Gao, Y. Zhu, J. Ding, Electrode-controlled confinement of conductive filaments in a nanocolumn embedded symmetric-asymmetric rram structure. J. Mater. Chem. C **8**(5), 1577–1582 (2020)
183. H. Seok, S. Son, S.B. Jathar, J. Lee, T. Kim, Synapse-mimetic hardware-implemented resistive random-access memory for artificial neural network. Sensors **23**(6), 3118 (2023)
184. F. Pan, S. Gao, C. Chen, C. Song, F. Zeng, Recent progress in resistive random access memories: Materials, switching mechanisms, and performance. Mater. Sci. Eng. R Rep. **83**, 1–59 (2014)
185. N. Arun, L.V. Sangani, K. Vinod Kumar, A. Mangababu, M.G. Krishna, A. Pathak, S. Nageswara Rao, Effects of swift heavy ion irradiation on the performance of hfo 2-based resistive random access memory devices. J. Mater. Sci. Mater. Electron. **32**, 2973–2986 (2021)
186. J.H. Heo, D.H. Shin, S.H. Moon, M.H. Lee, D.H. Kim, S.H. Oh, W. Jo, S.H. Im, Memory effect behavior with respect to the crystal grain size in the organic-inorganic hybrid perovskite nonvolatile resistive random access memory. Sci. Rep. **7**(1), 16586 (2017)
187. M. Arita, Y. Ohno, Y. Murakami, K. Takamizawa, A. Tsurumaki-Fukuchi, Y. Takahashi, Microstructural transitions in resistive random access memory composed of molybdenum oxide with copper during switching cycles. Nanoscale. **8**(31), 14754–14766 (2016)
188. J. Shen, P. Guan, A. Jiang, W. Fan, S. Li, Y. Liu, S. Xu, S. Cao, A polyanionic strategy to modify the perovskite grain boundary for a larger switching ratio in flexible woven resistive random-access memories. ACS Appl. Mater. Interfaces **14**(39), 44652–44664 (2022)
189. K. Zhang, Y. Ren, P. Ganesh, Y. Cao, Effect of electrode and oxide properties on the filament kinetics during electroforming in metal-oxide-based memories. npj Comput. Mater. **8**(1), 76 (2022)
190. D.S. Kuzmichev, Y.Y. Lebedinskii, C.S. Hwang, A.M. Markeev, Atomic layer deposited oxygen-deficient taox layers for electroforming-free and reliable resistance switching memory. Phys. Status Solidi (RRL)–Rapid Res. Lett. **12**(12), 1800429 (2018)
191. K. Egorov, Y.Y. Lebedinskii, A. Markeev, O. Orlov, Full ald ta2o5-based stacks for resistive random access memory grown with in vacuo xps monitoring. Appl. Surf. Sci. **356**, 454–459 (2015)
192. T.R. Desai, S.S. Kundale, T.D. Dongale, C. Gurnani, Evaluation of cellulose-mxene composite hydrogel based bio-resistive random access memory material as mimics for biological synapses. ACS Appl. Bio Mater. (2023)
193. D.P. Sahu, S.N. Jammalamadaka, Detection of bovine serum albumin using hybrid tio2+ graphene oxide based bio-resistive random access memory device. Sci. Rep. **9**(1), 1–10 (2019)
194. D. Mishra, K. Mokurala, A. Kumar, S.G. Seo, H.B. Jo, S.H. Jin, Light-mediated multi-level flexible copper iodide resistive random access memory for forming-free, ultra-low power data storage application. Adv. Funct. Mater. **33**(8), 2211022 (2023)
195. H. Jeong, J. Shin, S. Kim, J.J. Pak, Improved resistive switching characteristics by o2 plasma treatment in bi-layer ti/zno/opt-zno/ito rram. Curr. Appl. Phys. **49**, 120–126 (2023)
196. D. Bao, Transition metal oxide thin films for nonvolatile resistive random access memory applications. J. Ceram. Soc. Jpn. **117**(1369), 929–934 (2009)
197. J. Han, K. Park, H.-M. Kim, T.-S. Yoon, Tunable multilevel gate oxide capacitance and flat-band voltage shift characteristics by filament formation in double-floating-gate metal–oxide–semiconductor capacitors. Adv. Electron. Mater., 2201110 (2023)
198. N.C. Das, Y.-P. Kim, S.-M. Hong, J.-H. Jang, Effects of top and bottom electrodes materials and operating ambiance on the characteristics of mgfx based bipolar rrams. Nanomaterials **13**(6), 1127 (2023)
199. T. Chen, K. Leng, Z. Ma, X. Jiang, K. Chen, W. Li, J. Xu, L. Xu, Tracing the si dangling bond nanopathway evolution ina-sinx: H resistive switching memory by the transient current. Nanomaterials **13**(1), 85 (2023)
200. F. Eskandari, S. Porter, M. Venkatesan, P. Kameli, K. Rode, J. Coey, Magnetization and anisotropy of cobalt ferrite thin films. Phys. Rev. Mater. **1**(7), 074413 (2017)
201. C. Orozco, A. Melendez, S. Manadhar, S. Singamaneni, K.M. Reddy, K. Gandha, I. Niebedim, C.V. Ramana, Effect of molybdenum incorporation on the structure and magnetic properties of cobalt ferrite. J. Phys. Chem. C **121**(45), 25463–25471 (2017)
202. G.L. Jadhav, S. More, C. Kale, K. Jadhav, Effect of magnesium substitution on the structural, morphological, optical and wettability properties of cobalt ferrite thin films. Phys. B Condens. Matter **555**, 61–68 (2019)
203. M. Bastianello, S. Gross, M.T. Elm, Thermal stability, electrochemical and structural characterization of hydrothermally synthesised cobalt ferrite (cofe 2 o 4). RSC Adv. **9**(57), 33282–33289 (2019)
204. Y. Suzuki, G. Hu, R. Van Dover, R. Cava, Magnetic anisotropy of epitaxial cobalt ferrite thin films. J. Magn. Magn. Mater. **191**(1–2), 1–8 (1999)
205. T. Dhakal, D. Mukherjee, R. Hyde, P. Mukherjee, M. Phan, H. Srikanth, S. Witanachchi, Magnetic anisotropy and field switching in cobalt ferrite thin films deposited by pulsed laser ablation. J. Appl. Phys. **107**(5), 053914 (2010)
206. V. Kumbhar, A. Jagadale, N. Shinde, C. Lokhande, Chemical synthesis of spinel cobalt ferrite (cofe2o4) nano-flakes for supercapacitor application. Appl. Surf. Sci. **259**, 39–43 (2012)
207. Y.-Q. Chu, Z.-W. Fu, Q.-Z. Qin, Cobalt ferrite thin films as anode material for lithium ion batteries. Electrochim. Acta. **49**(27), 4915–4921 (2004)
208. A. Bagade, K. Rajpure, Development of cofe2o4 thin films for nitrogen dioxide sensing at moderate operating temperature. J. Alloys Compd. **657**, 414–421 (2016)
209. F.R. Mariosi, J. Venturini, A. Cas Viegas, C.P. Bergmann, Lanthanum-doped spinel cobalt ferrite (cofe2o4) nanoparticles for environmental applications. Ceram. Int. **46**(3), 2772–2779 (2020)
210. S.-B. Xia, W.-J. Huang, X. Shen, J. Liu, F.-X. Cheng, H. Guo, J.-J. Liu, Fabrication of porous ni/cofe2o4@ C composite for pseudocapacitive lithium storage. J. Alloys Compd. **854**, 157177 (2021)
211. M.A. Almessiere, Y.A. Slimani, M. Hassan, M.A. Gondal, E. Cevik, A. Baykal, Investigation of hard/soft cofe2o4/nisc0. 03fe1. 97o4 nanocomposite for energy storage applications. Int. J. Energy Res. **45**(11), 16691–16708 (2021)
212. S. Munjal, N. Khare, Electroforming free controlled bipolar resistive switching in al/cofe2o4/fto device with self-compliance effect. Appl. Phys. Lett. **112**(7), 073502 (2018)
213. A. Singh, A. Singh, S. Singh, P. Tandon, B. Yadav, Preparation and characterization of nanocrystalline nickel ferrite thin films for development of a gas sensor at room temperature. J. Mater. Sci. Mater. Electron. **27**, 8047–8054 (2016)
214. G. Rasic, J. Schwartz, Coercivity reduction in nickel ferrite (nife _{2} o _{4}) thin films through surface patterning. IEEE Magn. Lett. **5**, 1–4 (2014)
215. L. Wang, X. Li, J. Li, M. Liu, S. Xu, H. Li, Structural and electromagnetic properties of nialxfe2- xo4/sio2 nanocomposite films deposited using a sol-gel spin-coating method. J. Magn. Magn. Mater. **444**, 193–197 (2017)

216. S. Madake, K. Rajpure, Synergetic effect of thermal and electromagnetic energy on electrical properties of zinc ferrite thin film. Mater. Today Commun. **21**, 100641 (2019)
217. M. Vadiyar, S. Bhise, S. Patil, S. Patil, D. Pawar, A. Ghule, P. Patil, S. Kolekar, Mechanochemical growth of a porous znfe 2 o 4 nano-flake thin film as an electrode for supercapacitor application. RSC Adv. **5**(57), 45935–45942 (2015)
218. M. Qin, Q. Shuai, G. Wu, B. Zheng, Z. Wang, H. Wu, Zinc ferrite composite material with controllable morphology and its applications. Mater. Sci. Eng. B **224**, 125–138 (2017)
219. R. Tholkappiyan, K. Vishista, Synthesis and characterization of barium zinc ferrite nanoparticles: working electrode for dye sensitized solar cell applications. Sol. Energy **106**, 118–128 (2014)
220. M.H. Habibi, A.H. Habibi, M. Zendehdel, M. Habibi, Dye-sensitized solar cell characteristics of nanocomposite zinc ferrite working electrode: Effect of composite precursors and titania as a blocking layer on photovoltaic performance. Spectrochim. Acta A Mol. Biomol. Spectrosc. **110**, 226–232 (2013)
221. S. Al-Meer, Z.K. Ghouri, K. Elsaid, A. Easa, M.T. Al-Qahtani, M.S. Akhtar, Engineering of magnetically separable znfe2o4@ tio2 nanofibers for dye-sensitized solar cells and removal of pollutant from water. J. Alloys Compd. **723**, 477–483 (2017)
222. O.A. Onyedikachi, S.O. Aisida, A. Agbogu, I. Rufus, I. Ahmad, M. Maaza, F.I. Ezema, Zinc ferrite nanoparticles capped with gongronema latifolium for moderate hyperthermia applications. Appl. Phys. A **128**(2), 95 (2022)
223. Y. Yang, X. Liu, Y. Yang, W. Xiao, Z. Li, D. Xue, F. Li, J. Ding, Synthesis of nonstoichiometric zinc ferrite nanoparticles with extraordinary room temperature magnetism and their diverse applications. J. Mater. Chem. C **1**(16), 2875–2885 (2013)
224. F. Grasset, N. Labhsetwar, D. Li, D. Park, N. Saito, H. Haneda, O. Cador, T. Roisnel, S. Mornet, E. Duguet et al., Synthesis and magnetic characterization of zinc ferrite nanoparticles with different environments: powder, colloidal solution, and zinc ferrite- silica core- shell nanoparticles. Langmuir **18**(21), 8209–8216 (2002)
225. S. Jadhav, P. Hankare, R. Patil, R. Sasikala, Effect of sintering on photocatalytic degradation of methyl orange using zinc ferrite. Mater. Lett. **65**(2), 371–373 (2011)
226. S. Sharma, V. Dutta, P. Raizada, A. Hosseini-Bandegharaei, V. Thakur, V.-H. Nguyen, Q. VanLe, P. Singh et al., An overview of heterojunctioned znfe2o4 photocatalyst for enhanced oxidative water purification. J. Environ. Chem. Eng. **9**(5), 105812 (2021)
227. S. Piramanayagam, J. Moodera, R. Cowburn, R. Sbiaa, Focus on spintronics and spin physics. Phys. Status Solidi (RRL)–Rapid Res. Lett. **5**(12), 117–118 (2011)
228. A. Adiba, V. Pandey, T. Ahmad, P. Nehla, S. Munjal, Multilevel resistive switching with negative differential resistance in al/nio/znfe2o4/ito reram device. Phys. B Condens. Matter. **654**, 414742 (2023)
229. X. Yu, T. Shen, C. Zhu, Q. Zeng, A. Yu, S. Liu, R. Yi, Z. Weng, Y. Zhan, X. Hou et al., Memory devices via unipolar resistive switching in symmetric organic-inorganic perovskite nanoscale heterolayers. ACS Appl. Nano Mater. **3**(12), 11889–11896 (2020)
230. L. Zhong, L. Jiang, R. Huang, C. De Groot, Nonpolar resistive switching in cu/sic/au non-volatile resistive memory devices. Appl. Phys. Lett. **104**(9), 093507 (2014)
231. F.L. Aguirre, J. Suñé, E. Miranda, Spice implementation of the dynamic memdiode model for bipolar resistive switching devices. Micromachines **13**(2), 330 (2022)
232. G. Khurana, N. Kumar, M. Chhowalla, J.F. Scott, R.S. Katiyar, Non-polar and complementary resistive switching characteristics in graphene oxide devices with gold nanoparticles: Diverse approach for device fabrication. Sci. Rep. **9**(1), 1–10 (2019)
233. R. Deb, P. Pathak, S.R. Mohapatra, U. Das, Polarity independent resistive switching in mos2 nanosheets and peo based nanocomposite films. Jpn. J. Appl. Phys. (2022)
234. L. Michalas, S. Stathopoulos, A. Khiat, T. Prodromakis, Conduction mechanisms at distinct resistive levels of pt/tio2-x/pt memristors. Appl. Phys. Lett. **113**(14), 143503 (2018)
235. Y. Tao, X. Li, Z. Wang, G. Li, H. Xu, X. Zhao, Y. Lin, Y. Liu, Neutron irradiation-induced effects on the reliability performance of electrochemical metallization memory devices. J. Semicond. **42**(1), 014103 (2021)
236. K.-H. Kwon, D.-W. Kim, H.-J. Kim, S.-M. Jin, D.-S. Woo, S.-H. Park, J.-G. Park, An electroforming-free mechanism for cu 2 o solid-electrolyte-based conductive-bridge random access memory (cbram). J. Mater. Chem. C **8**(24), 8125–8134 (2020)
237. R. Soni, P. Meuffels, A. Petraru, M. Hansen, M. Ziegler, O. Vavra, H. Kohlstedt, D.S. Jeong, Bipolar switching polarity reversal by electrolyte layer sequence in electrochemical metallization cells with dual-layer solid electrolytes. Nanoscale **5**(24), 12598–12606 (2013)
238. W. Banerjee, W.F. Cai, X. Zhao, Q. Liu, H. Lv, S. Long, M. Liu, Intrinsic anionic rearrangement by extrinsic control: Transition of rs and crs in thermally elevated tin/hfo 2/pt rram. Nanoscale **9**(47), 18908–18917 (2017)
239. A. Roy, P.-R. Cha, Electric field induced charge migration and formation of conducting filament during resistive switching in electrochemical metallization (ecm) memory cells. J. Appl. Phys. **128**(20), 205102 (2020)
240. Y. Sun, C. Song, S. Yin, L. Qiao, Q. Wan, J. Liu, R. Wang, F. Zeng, F. Pan, Cluster-type filaments induced by doping in low-operation-current conductive bridge random access memory. ACS Appl. Mater. Interfaces **12**(26), 29481–29486 (2020)
241. Y. Yang, W. Lu, Nanoscale resistive switching devices: mechanisms and modeling. Nanoscale **5**(21), 10076–10092 (2013)
242. D. Ielmini, R. Bruchhaus, R. Waser, Thermochemical resistive switching: materials, mechanisms, and scaling projections. Phase Transit. **84**(7), 570–602 (2011)
243. A. Goswami, *Thin Film Fundamentals*. New age International, ??? (1996)
244. E. Brynjolfsson, A. Mcafee, Artificial intelligence, for real. Harv. Bus. Rev. **1**, 1–31 (2017)
245. S. Hanyu, The combination of metal oxides as oxide layers for rram and artificial intelligence. arXiv preprint arXiv:2305.00166 (2023)
246. S.-T. Wei, B. Gao, D. Wu, J.-S. Tang, H. Qian, H.-Q. Wu, Trends and challenges in the circuit and macro of rram-based computing-in-memory systems. Chip **1**(1), 100004 (2022)
247. H. An, J. Li, Y. Li, X. Fu, Y. Yi, Three dimensional memristor-based neuromorphic computing system and its application to cloud robotics. Comput. Electr. Eng. **63**, 99–113 (2017)
248. B. Mouttet et al., Memristor pattern recognition circuit architecture for robotics, in: *Proceedings of the 2nd International Multi-Conference on Engineering and Technological Innovation II*, (2009), pp. 65–70
249. J.K. Eshraghian, K. Cho, C. Zheng, M. Nam, H.H.-C. Iu, W. Lei, K. Eshraghian, Neuromorphic vision hybrid rram-cmos architecture. IEEE Trans. Very Large Scale Integr. (VLSI) Syst. **26**(12), 2816–2829 (2018)
250. S. Yu, B. Gao, Z. Fang, H. Yu, J. Kang, H.-S.P. Wong, A neuromorphic visual system using rram synaptic devices with sub-pj energy and tolerance to variability: Experimental characterization and large-scale modeling, in: *2012 International Electron Devices Meeting*, (IEEE, 2012), pp. 10–4
251. M. Chang, S.D. Spetalnick, B. Crafton, W.-S. Khwa, Y.-D. Chih, M.-F. Chang, A. Raychowdhury, A 40nm 60.64 tops/w ecc-capable compute-in-memory/digital 2.25 mb/768kb rram/sram system with embedded cortex m3 microprocessor for edge recommendation systems, in: *2022 IEEE International Solid-State Circuits Conference (ISSCC)*, vol. 65, (IEEE, 2022), pp. 1–3

252. Y. Lin, H. Wu, B. Gao, P. Yao, W. Wu, Q. Zhang, X. Zhang, X. Li, F. Li, J. Lu et al., Demonstration of generative adversarial network by intrinsic random noises of analog rram devices, in: *2018 IEEE International Electron Devices Meeting (IEDM)*, (IEEE, 2018), pp. 3–4
253. Z. Alamgir, K. Beckmann, J. Holt, N.C. Cady, Pulse width and height modulation for multi-level resistance in bi-layer tao x based rram. Appl. Phys. Lett. **111**(6), 063111 (2017)
254. U.B. Isyaku, M.H.B.M. Khir, I.M. Nawi, M. Zakariya, F. Zahoor, Zno based resistive random access memory device: a prospective multifunctional next-generation memory. IEEE Access **9**, 105012–105047 (2021)
255. A. Yousefi, N. Eslami, M.H. Moaiyeri, A reliable and energy-efficient nonvolatile ternary memory based on hybrid finfet/rram technology. IEEE Access **10**, 105040–105051 (2022)
256. I. Oh, J. Pyo, S. Kim, Resistive switching and synaptic characteristics in zno/taon-based rram for neuromorphic system. Nanomaterials **12**(13), 2185 (2022)
257. G. Charan, J. Hazra, K. Beckmann, X. Du, G. Krishnan, R.V. Joshi, N.C. Cady, Y. Cao, Accurate inference with inaccurate rram devices: Statistical data, model transfer, and on-line adaptation, in: *2020 57th ACM/IEEE Design Automation Conference (DAC)*, (IEEE, 2020), pp. 1–6
258. W. Shim, Y. Luo, J.-S. Seo, S. Yu, Investigation of read disturb and bipolar read scheme on multilevel rram-based deep learning inference engine. IEEE Trans. Electron Devices. **67**(6), 2318–2323 (2020)
259. V. Milo, A. Glukhov, E. Perez, C. Zambelli, N. Lepri, M.K. Mahadevaiah, E.P.-B. Quesada, P. Olivo, C. Wenger, D. Ielmini, Accurate program/verify schemes of resistive switching memory (rram) for in-memory neural network circuits. IEEE Trans. Electron Devices **68**(8), 3832–3837 (2021)
260. Q. Wang, X. Wang, S.H. Lee, F.-H. Meng, W.D. Lu, A deep neural network accelerator based on tiled rram architecture, in: *2019 IEEE International Electron Devices Meeting (IEDM)*, (IEEE, 2019), pp. 14–4
261. B. Sueoka, A.Y. Vicenciodelmoral, M.M.H. Tanim, X. Zhao, F. Zhao, Correlation of natural honey-based rram processing and switching properties by experimental study and machine learning. Solid State Electron **197**, 108463 (2022)
262. D. Kumar, S. Shrivastava, A. Saleem, A. Singh, H. Lee, Y.-H. Wang, T.-Y. Tseng, Highly efficient invisible tao x/zto bilayer memristor for neuromorphic computing and image sensing. ACS Appl. Electron. Mater. **4**(5), 2180–2190 (2022)
263. A. Vitale, A. Renner, C. Nauer, D. Scaramuzza, Y. Sandamirskaya, Event-driven vision and control for uavs on a neuromorphic chip, in: *2021 IEEE International Conference on Robotics and Automation (ICRA)*, pp. 103–109 (2021). IEEE
264. I.-A. Fyrigos, V. Ntinas, N. Vasileiadis, G.C. Sirakoulis, P. Dimitrakis, Y. Zhang, I.G. Karafyllidis, Memristor crossbar arrays performing quantum algorithms. IEEE Trans. Circuits Syst. I Regul. Pap. **69**(2), 552–563 (2021)
265. Z. Chen, Y. Yu, L. Jin, Y. Li, Q. Li, T. Li, J. Li, H. Zhao, Y. Zhang, H. Dai et al., Broadband photoelectric tunable quantum dot based resistive random access memory. J. Mater. Chem. C **8**(6), 2178–2185 (2020)
266. K. Portner, M. Schmuck, P. Lehmann, C. Weilenmann, C. Haffner, P. Ma, J. Leuthold, M. Luisier, A. Emboras, Analog nanoscale electro-optical synapses for neuromorphic computing applications. ACS Nano **15**(9), 14776–14785 (2021)
267. J. Shen, Z. Cheng, P. Zhou, Optical and optoelectronic neuromorphic devices based on emerging memory technologies. Nanotechnology (2022)
268. Z. Jin, L. Yang, S. Shi, T. Wang, G. Duan, X. Liu, Y. Li, Flexible polydopamine bioelectronics. Adv. Funct. Mater. **31**(30), 2103391 (2021)
269. C. Zhang, Y. Li, C. Ma, Q. Zhang, Recent progress of organic-inorganic hybrid perovskites in rram, artificial synapse, and logic operation. Small Sci. **2**(2), 2100086 (2022)
270. M. Ismail, C. Mahata, S. Kim, Electronic synaptic plasticity and analog switching characteristics in pt/tiox/alox/altaon/tan multilayer rram for artificial synapses. Appl. Surf. Sci. **599**, 153906 (2022)
271. D. Liu, H. Yu, Y. Chai, Low-power computing with neuromorphic engineering. Adv. Intell. Syst. **3**(2), 2000150 (2021)
272. H. Li, S. Wang, X. Zhang, W. Wang, R. Yang, Z. Sun, W. Feng, P. Lin, Z. Wang, L. Sun et al., Memristive crossbar arrays for storage and computing applications. Adv. Intell. Syst. **3**(9), 2100017 (2021)
273. X. Ji, X. Zhao, M.C. Tan, R. Zhao, Artificial perception built on memristive system: Visual, auditory, and tactile sensations. Adv. Intell. Syst. **2**(3), 1900118 (2020)
274. F. Li, R. Wang, C. Song, M. Zhao, H. Ren, S. Wang, K. Liang, D. Li, X. Ma, B. Zhu et al., A skin-inspired artificial mechanoreceptor for tactile enhancement and integration. ACS Nano **15**(10), 16422–16431 (2021)
275. W. Wang, E. Covi, A. Milozzi, M. Farronato, S. Ricci, C. Sbandati, G. Pedretti, D. Ielmini, Neuromorphic motion detection and orientation selectivity by volatile resistive switching memories. Adv. Intell. Syst. **3**(4), 2000224 (2021)
276. S. Zhu, B. Sun, G. Zhou, C. Ke, T. Guo, H. Zhao, F. Yang, Y. Zhang, Y. Wu, Y. Zhao, A flexible resistive switching device for logical operation applications in wearable systems. Mater. Today Chem. **26**, 101169 (2022)
277. R. Govindaraj, S. Ghosh, S. Katkoori, Csro-based reconfigurable true random number generator using rram. IEEE Trans. Very Large Scale Integr. (VLSI) Syst. **26**(12), 2661–2670 (2018)
278. J. Yang, Y. Lin, Y. Fu, X. Xue, B. Chen, A small area and low power true random number generator using write speed variation of oxidebased rram for iot security application, in: *2017 IEEE International Symposium on Circuits and Systems (ISCAS)*, (IEEE, 2017), pp. 1–4
279. S. Singh, F. Zahoor, G. Rajendran, V. Rana, S. Patkar, A. Chattopadhyay, F. Merchant, Integrated architecture for neural networks and security primitives using rram crossbar. arXiv preprint arXiv:2304.13531 (2023)
280. M.B. Zefrei, T. Asbaghi, M. Khosraviani, A novel circuit level polymorphism for hardware watermarking to intellectual property protection. J. Soft Comput Decis. Support Syst. **8**(4), 11–15 (2021)
281. W. Li, S. Huang, X. Sun, H. Jiang, S. Yu, Secure-rram: A 40nm 16kb compute-in-memory macro with reconfigurability, sparsity control, and embedded security, in: *2021 IEEE Custom Integrated Circuits Conference (CICC)*, (IEEE, 2021), pp. 1–2
282. B. Yang, D. Arumí, S. Manich, Á. Gómez-Pau, R. Rodríguez-Montañés, M.B. González, F. Campabadal, L. Fang, Serial rram cell for secure bit concealing. Electronics **10**(15), 1842 (2021)
283. M.N.I. Khan, S. Ghosh, Comprehensive study of security and privacy of emerging non-volatile memories. J. Low Power Electron. Appl. **11**(4), 36 (2021)
284. Y. Pang, H. Wu, B. Gao, N. Deng, D. Wu, R. Liu, S. Yu, A. Chen, H. Qian, Optimization of rram-based physical unclonable function with a novel differential read-out method. IEEE Electron Device Lett. **38**(2), 168–171 (2017)
285. G.S. Lee, G.-H. Kim, K. Kwak, D.S. Jeong, H. Ju, Enhanced reconfigurable physical unclonable function based on stochastic nature of multilevel cell rram. IEEE Trans. Electron Devices **66**(4), 1717–1721 (2019)
286. A. Chen, Comprehensive assessment of rram-based puf for hardware security applications, in: *2015 IEEE International Electron Devices Meeting (IEDM)*, (IEEE, 2015), pp. 10–7

Authors and Affiliations

Ketankumar Gayakvad[1,6] · **Kaushik Somdatta**[2] · **Vikas Mathe**[3] · **Tukaram Dongale**[4] · **Madhuri W**[5] · **Ketaki Patankar**[6,7]

Kaushik Somdatta
sdkaushik@csr.res.in

Vikas Mathe
vikasmathe@gmail.com

Tukaram Dongale
tdd.snst@unishivaji.ac.in

Madhuri W
madhuriw12@gmail.com

Ketaki Patankar
ketakiketan@gmail.com

[1] Department of Physics, K. J. Somaiya College of Science and Commerce, Vidyavihar, Mumbai, Maharashtra 400077, India

[2] UGC-DAE Consortium for Scientific Research, Mumbai Centre, Room No.61, R-5 Shed, BARC Campus, Mumbai, Maharashtra 400085, India

[3] Novel Material Research Laboratory, Savitribai Phule Pune University, Ganeshkhind, Pune, Maharashtra 411007, India

[4] Computational Electronics and Nanoscience Research Laboratory, School of Nanoscience and Technology, Vidyanagar, Shivaji University, Kolhapur, Maharashtra 416 004, India

[5] Centre for Functional Materials, Vellore Institute of Technology, Vellore, Tamil Nadu 632014, India

[6] Composite Materials Laboratory, Rajaram College, Vidyanagar, Kolhapur, Maharashtra 416 004, India

[7] Department of Physics, Ismail Yusuf College of Arts, Science and Commerce, Hardevi Society, Natwar Nagar, Jogeshwari East, Mumbai, Maharashtra 400060, India